Target normal single-spin asymmetry in inclusive electron-nucleon scattering in the $1/N_c$ expansion

J. L. Goity,[1,2,*] C. Weiss,[2,†] and C. Willemyns[3,‡]

[1]*Department of Physics, Hampton University, Hampton, Virginia 23668, USA*
[2]*Theory Center, Jefferson Lab, Newport News, Virginia 23606, USA*
[3]*Service de Physique Nucléaire et Subnucléaire, Université de Mons, UMONS Research Institute for Complex Systems, Place du Parc 20, 7000 Mons, Belgium*

(Received 24 March 2023; accepted 2 May 2023; published 22 May 2023)

The target normal single-spin asymmetry in inclusive electron-nucleon scattering is studied in the low-energy regime that includes the Δ resonance. The particular interest in the asymmetry resides in that it is driven by two-photon exchange effects. It probes the spin-dependent absorptive part of the two-photon exchange amplitude, which is free of infrared and collinear singularities and represents the most pristine expression of two-photon exchange dynamics. The study presented here uses the $1/N_c$ expansion of QCD, which combines the N and Δ through the emergent $SU(4)$ spin-flavor symmetry in the baryon sector and allows for a systematic construction of the transition electromagnetic (EM) currents. The analysis includes the first subleading corrections in the $1/N_c$ expansion and presents results for elastic and inelastic final states. The asymmetry is found to be in the range $10^{-3} - 10^{-2}$. The Δ resonance plays an important role as an intermediate state in the elastic asymmetry and as a final state in the inclusive asymmetry.

DOI: 10.1103/PhysRevD.107.094026

I. INTRODUCTION

The electromagnetic (EM) interaction is a fundamental tool for the study of hadronic structure and dynamics. In general, the processes involved have been traditionally analyzed at the leading order in the electromagnetic interaction. In electron-hadron scattering this is $\mathcal{O}(\alpha_{\rm em})$, the so-called one-photon exchange approximation (OPE). In hadronic observables there are however important effects that require the consideration of genuine higher order EM interactions, such as the isospin breaking in hadronic masses, e.g., the mass difference between the charged and neutral pions that is almost entirely due to EM, and the important contribution to the proton-neutron mass difference where the EM contribution is of similar magnitude to the one due to the isospin breaking by the quark masses. In electron scattering, the subleading EM contributions due to two-photon exchange (TPE) have been identified as the likely source of the discrepancy observed in the OPE approximation extraction of the ratio G_E^p/G_M^p from measurements using the Rosenbluth separation versus the polarization transfer methods [1–3]. Measurements that expose the TPE effects are thus of particular interest. One of them consists in the comparison of the cross sections of electron and positron scattering on the proton, such as the recent experiments at DESY [4,5] and possible future experiments at Jefferson Lab [6]. In addition, observables in parity-violating electron scattering receive corrections from TPE [7]. In general the theoretical study of the TPE effects is affected by significant uncertainties as it requires knowledge of EM hadronic structure beyond the EM form factors, namely the doubly virtual photon Compton amplitudes, and is thus still a work in progress.

A particularly interesting TPE effect is the transverse target single-spin asymmetry (TSSA) in electron-nucleon scattering with quasi-two-body final states, i.e., elastic scattering $e + N \to e' + N$ or inclusive scattering $e + N \to e' + X$. If the target nucleon is polarized transversely to the scattering plane, the cross section generally depends on the scalar product of the spin vector and the normal vector of the plane. Due to P and T invariance, such a spin dependence can arise only from TPE, because it requires a nonzero absorptive part of the electron-nucleon EM scattering amplitude [8]. The spin-dependent cross section produced in this way is given by on-shell matrix elements of the EM current, is free of collinear and infrared divergences, and can be considered independently of radiative corrections related to real photon emission into the final state. These features make the TSSA the most

*goity@jlab.org
†weiss@jlab.org
‡cintiawillemyns@gmail.com

unambiguous TPE effect in electron scattering. (The same TPE mechanism gives rise to a beam single-spin asymmetry in the case of transverse electron polarization; this effect is proportional to the electron mass and generally much smaller than the TSSA; see discussion in Sec. V.)

The TSSA in elastic eN scattering has been studied theoretically in Refs. [9–12], and more recently in Refs. [13,14], using hadronic physics methods. This asymmetry is expected to be of the order $\sim 10^{-2}$ for momentum transfers $Q^2 \lesssim 1\ \mathrm{GeV}^2$. Experiments performed with recoil polarization in ep elastic scattering obtained values consistent with zero; see [15] and references therein. Further tests will become possible with contemporary elastic scattering experiments.

The TSSA in inclusive eN scattering has been analyzed in deep-inelastic kinematics in Refs. [16–19] using a partonic picture and various assumptions regarding QCD interactions. These calculations predict values in the range $10^{-4} - 10^{-3}$, substantially smaller than the elastic TSSA. Measurements in DIS kinematics have been performed with a proton target at HERMES at 27.5 GeV beam energy [20], and with a ^{3}He target at Jefferson Lab Hall A with beam energies 2.4, 3.6, and 5.9 GeV [21–23]. A next-generation measurement with proton target and electron and positron beams with energies from 2.2 to 6.6 GeV has been proposed at Jefferson Lab [24].

A question of great interest is the behavior of the TSSA in inclusive eN scattering in the first resonance region, where the Δ isobar can appear both as an intermediate state in the TPE amplitude and as a final state in inelastic scattering. This region lies between the domain of elastic scattering at low energies and that of deep-inelastic scattering at high energies. If one understands the behavior of the TSSA in the resonance region, then one could follow its evolution with energy, connect the elastic and deep-inelastic domains, and explain the different orders of magnitude predicted for the two regions. Little is presently known about the inclusive TSSA in the resonance region from either theory or experiment. Measurements could be performed in electron scattering with energies $\sim$0.5–1.5 GeV, perhaps at the lower end of the proposed experiment of Ref. [24] or in future dedicated experiments.

The elastic TSSA in the resonance region can be calculated in terms of the empirical electroproduction amplitudes extracted from eN scattering data; see Ref. [25] and references therein. Theoretical uncertainties are significant, as the effect is sensitive to the phases and arises as a sum over contributions of comparable size and varying sign. The inelastic or inclusive TSSA in the resonance region is much more difficult to calculate as it requires also amplitudes such as $\Delta \to \Delta$, which cannot be measured in eN scattering. In addition to the Δ it can also receive contributions from nonresonant πN final states. This calls for a theoretical framework that can organize the hadronic intermediate/final states and predict the EM transition amplitudes.

The $1/N_c$ expansion organizes hadron structure and reactions on the basis of the scaling behavior in the number of colors in QCD [26,27]. It is particularly useful for baryons and permits a unified description of the N and Δ. In the large-N_c limit the baryon sector of QCD develops a dynamical spin-flavor symmetry $SU(2N_f)$, with $N_f = 2$ as the number of light flavors here [28–32]. N and Δ belong to the $SU(4)$ totally symmetric irreducible representation with $I = S = \frac{1}{2}, \ldots, \frac{N_c}{2}$, where I and S are the baryon's isospin and spin. $N \to N$, $N \to \Delta$, and $\Delta \to \Delta$ transition matrix elements are thus related by the $SU(4)$ symmetry. A systematic $1/N_c$ expansion of the EM transition currents can be performed, including subleading corrections, with all parameters fixed by the nucleon sector. A parametric distinction between resonant Δ and nonresonant πN states appears, with the latter relegated to subleading level. These features of the $1/N_c$ expansion allow one to develop an efficient framework for the present purpose.

In this work the TSSA in low-energy electron-nucleon scattering with TPE is analyzed using the $1/N_c$ expansion. The study covers the energy region below and above the Δ excitation threshold and considers the TSSA for both elastic scattering $eN \to e'N$ and inclusive scattering $eN \to e'X$, $X = N, \Delta$. The application of the $1/N_c$ expansion to the kinematic variables of electron scattering is discussed, and versions of the expansion appropriate in the different kinematic regimes are defined. Using the $1/N_c$ expansion of the EM current operators and their matrix elements between N and Δ states, the TSSA resulting from TPE is computed to first subleading order in $1/N_c$. The TSSA is evaluated numerically, and the contributions of Δ isobars as intermediate states (in elastic or inclusive scattering) and final states (in inclusive scattering) are quantified. Possible extensions of the techniques to the beam spin asymmetry and other observables in low-energy eN scattering are discussed.

In the regime of interest one can identify a low-energy domain below the onset of the Δ resonance, where only the elastic contribution in the TPE amplitude is present (the low-energy πN continuum contributes only beyond the order in $1/N_c$ considered here); a low-energy domain above the Δ resonance, where elastic and inelastic channels are open; and an intermediate energy domain that extends from the Δ resonance up to the onset of the higher resonances. Because the photon virtualities in the TPE amplitude cover a broad range (limited only by the c.m. energy of the eN collision), the form factors of the baryon EM currents play an important role. It is shown that they dramatically affect the contributions of the Δ resonance to the TSSA. This underscores the need of a systematic treatment of the transition currents as provided by the $1/N_c$ expansion.

The article is organized as follows: Sec. II summarizes the general methods for describing the target spin dependence of eN scattering and implementing the $1/N_c$ expansion in the baryon sector. Section III describes the application of the $1/N_c$ expansion in the different kinematic regions, construction of the one- and two-photon exchange amplitudes, and calculation of the TSSA. Section IV presents the numerical results and compares the contributions of various intermediate/final states. Section V discusses the significance of the results and possible extensions of the methods. Appendices A–E summarize technical material supporting the calculations, including the $SU(4)$ spin-flavor symmetry, the integrals appearing in the $1/N_c$ expansion of the TSSA, the results for the spin-independent and dependent cross sections, and the treatment of the Δ width.

II. METHODS

A. Target spin dependence in inclusive electron scattering

This work considers the process of inclusive scattering of an unpolarized electron on a transversely polarized nucleon,

$$e(k_{\rm i}) + N\uparrow(p_{\rm i}) \to e(k_{\rm f}) + X, \tag{1}$$

where $X = N, \pi N, \ldots$ denotes the hadronic final states accessible at the incident energy. In the regime to be studied here the inelastic final states are πN and dominated by the decay of the Δ resonance (as explained below), and the contributions of elastic and inelastic final states will be analyzed separately in the following. The 4-momentum transfer is given by

$$q \equiv k_{\rm i} - k_{\rm f} = p_{\rm f} - p_{\rm i}, \tag{2}$$

and the process is characterized by the invariants

$$s \equiv (k_{\rm i} + p_{\rm i})^2, \quad t \equiv q^2, \quad M_X^2 = (q + p_{\rm i})^2 = p_{\rm f}^2. \tag{3}$$

The differential cross section can be represented as [17]

$$\frac{d\sigma}{d\Gamma_{\rm f}} = \frac{d\sigma_U}{d\Gamma_{\rm f}} + e_N^\mu a_\mu \frac{d\sigma_N}{d\Gamma_{\rm f}}, \tag{4}$$

where $d\Gamma_{\rm f}$ is the invariant phase space of the final electron. The first term in Eq. (4) is the unpolarized cross section and the second one results from the effect of the polarization of the target nucleon. a^μ is the spin four-vector of the target nucleon, and e_N^μ is the normalized spacelike four-pseudovector given by

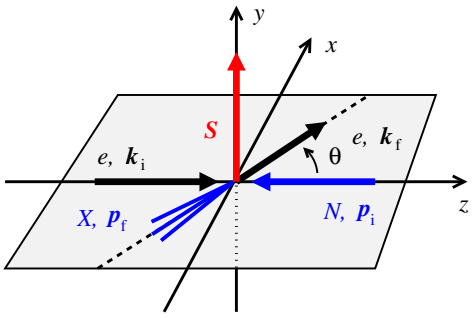

FIG. 1. Inclusive electron-nucleon scattering in the electron-nucleon c.m. frame. The nucleon is polarized in the direction normal to the scattering plane.

$$e_N^\mu \equiv \frac{N^\mu}{\sqrt{-N^2}}, \qquad N^\mu \equiv \epsilon^{\mu\alpha\beta\gamma} p_{{\rm i}\alpha} k_{{\rm i}\beta} k_{{\rm f}\gamma},$$
$$N^2 = \frac{t}{4}[st + (s - m_N^2)(s - M_X^2)]. \tag{5}$$

The quasi-two-body scattering process Eq. (1) can be viewed in reference frames where the 3-momenta (boldface fonts are used for spatial vectors) $\boldsymbol{k}_{\rm i}, \boldsymbol{k}_{\rm f}$, and $\boldsymbol{p}_{\rm i}$ lie in a plane, e.g., the target nucleon rest frame ($\boldsymbol{p}_{\rm i} = 0$), the electron-nucleon c.m. frame ($\boldsymbol{p}_{\rm i} + \boldsymbol{k}_{\rm i} = 0$), or the virtual photon-nucleon c.m. frame ($\boldsymbol{p}_{\rm i} + \boldsymbol{k}_{\rm i} - \boldsymbol{k}_{\rm f} = 0$). In such a frame the vector $\boldsymbol{e}_N$ is normal to the scattering plane (see Fig. 1) and given by

$$e_N = (0, \boldsymbol{e}_N), \qquad \boldsymbol{e}_N = \frac{\boldsymbol{k}_{\rm i} \times \boldsymbol{k}_{\rm f}}{|\boldsymbol{k}_{\rm i} \times \boldsymbol{k}_{\rm f}|}, \tag{6}$$

where m_N is the nucleon mass. The cross section Eq. (4) thus depends on the normal component of the nucleon spin. The target normal single-spin asymmetry is defined as the ratio

$$A_N \equiv \frac{d\sigma_N}{d\Gamma_{\rm f}} \Big/ \frac{d\sigma_U}{d\Gamma_{\rm f}}. \tag{7}$$

It can be measured either as the asymmetry of the cross sections with the nucleon polarized up and down for the same scattered electron momentum (up-down asymmetry), or as the asymmetry of the cross sections with the electron scattered to the left and to the right for the same nucleon polarization (left-right asymmetry).

The following theoretical analysis uses the electron-nucleon c.m. frame, where the 3-momenta in the initial and final states are $\boldsymbol{p}_{\rm i} = -\boldsymbol{k}_{\rm i}$, $\boldsymbol{p}_{\rm f} = -\boldsymbol{k}_{\rm f}$ (see Fig. 1). They are related to the invariants by

$$|\boldsymbol{k}_{\rm i}| = \frac{s - m_N^2}{2\sqrt{s}}, \qquad |\boldsymbol{k}_{\rm f}| = \frac{s - M_X^2}{2\sqrt{s}},$$
$$t = -2|\boldsymbol{k}_{\rm f}||\boldsymbol{k}_{\rm i}|(1 - \cos\theta), \tag{8}$$

where $\theta \equiv \text{angle}(\boldsymbol{k}_\text{f}, \boldsymbol{k}_\text{i})$ is the scattering angle. The expressions in the following do not refer to any specific coordinate system but are formulated in terms of abstract three-vector products in this frame.

B. $1/N_c$ expansion

The $1/N_c$ expansion is a powerful method for organizing hadron structure and reactions on the basis of the scaling behavior in the number of colors in QCD. The expansion needs definition, as it results from comparing QCD with varying number of degrees of freedom and allows for choices of the scaling behavior of the parameters of the theory (scale parameter, number of flavors, quark masses). The commonly adopted version, which works best for the phenomenology of the real world with $N_c = 3$ and two or three light flavors, is the 't Hooft expansion, where the number of flavors is fixed and particular physical observables (e.g., for $N_f = 2$, the ρ and the π meson masses) are used to define the quark masses and the QCD scale. The expansion can furthermore be implemented at the hadronic level by identifying the N_c scaling of the different quantities. That implementation can be made into a systematic $1/N_c$ expansion, in particular in the context of effective theories.

The $1/N_c$ expansion is particularly useful in the baryon sector of QCD; see Ref. [33] and references therein. The baryon masses are $\mathcal{O}(N_c)$, and the πN interaction is $\mathcal{O}(\sqrt{N_c})$. The latter requires for consistency that in the large-N_c limit the baryon sector develops a dynamical contracted spin-flavor symmetry described by the $SU(2N_f)$ group, or $SU(4)$ for $N_f = 2$ [28–30]. In the rest frame of the baryons, the 15 generators of $SU(4)$ can be identified with the spin $\hat{S}^i$, isospin $\hat{I}^a$, and spin-flavor $\hat{G}^{ia}$ operators (see Appendix A). In frames where the baryons have momenta $\mathcal{O}(N_c^0)$, their velocities are $\mathcal{O}(N_c^{-1})$, because the masses are $\mathcal{O}(N_c)$, and their motion is effectively nonrelativistic. Transition matrix elements between baryon states in frames where the momenta are $\mathcal{O}(N_c^0)$ can therefore be computed in a nonrelativistic expansion, where they are expressed in terms of the $SU(4)$ generators and the initial/final baryon momenta.

The ground-state baryons belong to the totally symmetric $SU(4)$ multiplet. It consists of states with isospin/spin $I = S$ and $S = \frac{1}{2}, \ldots, \frac{N_c}{2}$, which includes the N and Δ states with $I = S = \frac{1}{2}$ and $\frac{3}{2}$. States in the multiple are characterized by S and the projections S_3 and I_3 and denoted by $|SS_3I_3\rangle$. The mass splitting between the states is $\mathcal{O}(N_c^{-1})$. In this multiplet the generators $\hat{G}^{ia}$ have matrix elements $\mathcal{O}(N_c)$ between states with $S = \mathcal{O}(N_c^0)$, while the generators $\hat{I}^a$ and $\hat{S}^i$ obviously have matrix elements $\mathcal{O}(N_c^0)$.

This work requires the matrix elements of the EM current operators between baryon states in the ground state multiplet. The assignment of electric charges to the quarks at arbitrary N_c [34] can be made in such a way that the Standard Model gauge and gravitational anomalies vanish as required for consistency, and such that the charges of the baryons are simply given by the usual relation $Q = 1/2 + \hat{I}^3$, independent of N_c. The quark charges are then given by $Q_q = \frac{3}{2N_c} + I_3$. In the following the current is considered for transitions between baryon states with 3-momenta $\boldsymbol{p}, \boldsymbol{p}' = \mathcal{O}(N_c^0)$, and generally different spins $S' \neq S$, and therefore different masses; the 4-momentum transfer is $q \equiv p' - p$, and its components are $\boldsymbol{q} = \mathcal{O}(N_c^0)$ and $q^0 = \mathcal{O}(N_c^{-1})$. Including leading and subleading terms in the $1/N_c$ expansion, the isoscalar (S) and isovector (V) components of the EM current are given by [34][1]

$$J^\mu_S(q) = G^S_E(q^2)\frac{1}{2}g^{\mu 0} - i\frac{1}{2}\frac{G^S_M(q^2)}{\Lambda}\epsilon^{0\mu ij}q^i\hat{S}^j, \quad (9)$$

$$J^{\mu a}_V(q) = G^V_E(q^2)\hat{I}^a g^{\mu 0} - i\frac{6}{5}\frac{G^V_M(q^2)}{\Lambda}\epsilon^{0\mu ij}q^i\hat{G}^{ja}, \quad (10)$$

$$J^\mu_\text{EM}(q) = J^\mu_S(q) + J^{\mu 3}_V(q), \quad (11)$$

where $G^S_{E,M}$ and $G^V_{E,M}$ are the form factors of the electric and magnetic components.[2] The currents are expressed in terms of the $SU(4)$ spin-flavor generators and understood to be evaluated between multiplet states $\langle S'S'_3I'_3|\ldots|SS_3I_3\rangle$. The magnetic terms are written with a generic mass scale $\Lambda = \mathcal{O}(N_c^0)$, whose value is identified with the physical nucleon mass (exempt from N_c scaling); this formulation is natural for the $1/N_c$ expansion and avoids the appearance of spurious powers of N_c that would come from using the scaling m_N in the denominator. The form factors in Eqs. (9) and (10) are defined such that they coincide with the physical nucleon form factors for $\Lambda = m_N(\text{physical})$ and $N_c = 3$. In particular, the factor $6/5$ in the magnetic term of the isovector current was introduced such that, for $N_c = 3$, G^V_M coincides with the physical nucleon isovector magnetic form factor.

The currents given by Eqs. (9) and (10) satisfy current conservation to the necessary accuracy in $1/N_c$. For the magnetic terms (spatial components), this follows from the vector product structure of the vertices; for the electric terms (time components), it is realized because $q^0 = \mathcal{O}(N_c^{-1})$.

[1]Terms in the currents with higher powers of momenta have been neglected, such as the isovector contribution to the time component, which stems from a relativistic correction and is proportional to $\frac{1}{m_N\Lambda}\epsilon^{0ijk}q^i p^j \hat{G}^{ka}$. Such terms are suppressed except at the upper end of the energy domain considered here and are subleading in $1/N_c$. The electric quadrupole component of the current, which mediates $N - \Delta$ transitions, is suppressed by a factor $1/N_c^2$ with respect to the leading term [35] and thus irrelevant to the present calculation.

[2]For the sake of convenience in the calculations and without significant difference the G_E form factor is taken to be equal to the corresponding F_1 rather than the Sachs form factor.

The order in $1/N_c$ of the components of the currents in Eqs. (9) and (10) is as follows. The isovector magnetic current is $\mathcal{O}(N_c)$, being represented by the spin-flavor operator $\hat{G}^{ia}$ that has matrix elements $\mathcal{O}(N_c)$. This reflects the fact that the nucleon anomalous magnetic moment is $\mathcal{O}(N_c)$. (In the quark picture of baryons, this happens because the magnetic moments of the quarks add up coherently to form the total magnetic moment of the baryon, see for instance Ref. [36].) The remaining terms in the current are $\mathcal{O}(N_c^0)$, being proportional to the operators $\hat{1}, \hat{S}^i$, and I^a that have matrix elements $\mathcal{O}(N_c^0)$. At leading order in the $1/N_c$ expansion, the dominant current component is therefore the isovector magnetic current proportional to the operator $\hat{G}^{ia}$. Clear evidence of this dominance is the ratio of the isovector and isoscalar magnetic moments of the nucleon, $G_M^V(0)/G_M^S(0) = \mathcal{O}(N_c) = 5.34$. The dominant isovector magnetic current also induces the M_1 transitions $N \to \Delta$; the other current components only have matrix elements between states with same spin/isospin.

Equations (9) and (10) capture the $1/N_c$ expansion of the EM currents to the accuracy needed in the present calculation. Higher-order corrections beyond that accuracy arise from the nonrelativistic expansion of the motion of the baryons. For momenta $\mathcal{O}(N_c^0)$, both the spatial components of the convection current and the time component of the magnetic currents are $\mathcal{O}(N_c^{-1})$. Further higher-order corrections arise from the contribution of subleading spin-flavor operators, namely $\hat{S}^i\hat{\vec{S}}^2$ for the isoscalar magnetic current, and $\{\hat{G}^{i3}, \hat{S}^2\}$ and $\hat{S}^i\hat{I}^3$ for the isovector one. These higher-body spin-flavor operators are accompanied by factors $1/N_c^{n-1}$, where n is the number of spin-flavor generator factors in the composite operator [31,37]. The corrections to the magnetic currents are therefore suppressed by $\mathcal{O}(N_c^{-2})$ relative to the dominant isovector magnetic current. To the accuracy of the present calculation, these higher order terms in the currents are therefore irrelevant.

The momentum dependence of the form factors plays an essential role in the present calculation. The scale governing the momentum dependence of the form factors—the baryon "size" in the large-N_c limit—is $\mathcal{O}(N_c^0)$, and the momentum transfer is $t = \mathcal{O}(N_c^0)$, so that the functions are evaluated in a region where they differ significantly from their values at zero momentum transfer. The form factors in Eqs. (9) and (10) can be determined by matching the expressions for $N_c = 3$ with the empirical proton and neutron form factors, which gives

$$G_E^{S,V}(t) = G_E^p(t) \pm G_E^n(t),$$
$$G_M^{S,V}(t) = G_M^p(t) \pm G_M^n(t). \tag{12}$$

In the calculations and for the sake of obtaining analytical results, the small contribution of the neutron's electric form factor is neglected for simplicity, i.e., $G_E^n \equiv 0$, or equivalently $G_E^S = G_E^V = G_E^p$. This is further justified at the end of Sec. III A. Furthermore, it is assumed that the t dependence of all the form factors is of the dipole form with a common mass scale $\Lambda_{\rm EM}^2 = 0.71\ \mathrm{GeV}^2$, which in the domain of the present calculations is a standard and accurate parametrization [38].

The construction of the currents Eqs. (9) and (10) demonstrates the predictive power of the $1/N_c$ expansion. The structure is dictated by the spin-flavor symmetry in the large-N_c limit. The coefficients are fixed by observables measured in $N \to N$ transitions. Together, this then predicts the matrix elements of the same operator for $N \to \Delta$ and $\Delta \to \Delta$ transitions.

III. CALCULATION

A. Kinematic regimes for the $1/N_c$ expansion

In this work the $1/N_c$ expansion is used to study the spin dependence of inclusive eN scattering Eq. (1). When applying the $1/N_c$ expansion to the scattering process, it is necessary to specify the parametric order in $1/N_c$ of the kinematic variables—the scattering energy, momentum transfer, and final-state mass, Eq. (3). The physical scales for the scattering energy and final-state mass are set by the excitation energy of the Δ and N^* baryon resonances, which are of the parametric order

$$m_\Delta - m_N = \mathcal{O}(N_c^{-1}), \tag{13}$$

$$m_{N*} - m_N = \mathcal{O}(N_c^0). \tag{14}$$

Another physical scale arises from the excitation energy of nonresonant πN states, namely $m_{\pi N} - m_N$; this scale permits various choices for the assignment of its $1/N_c$ scaling (see below). How the scattering energy is chosen relative to the scales Eq. (14) determines what channels are open in the process, and how the $1/N_c$ expansion is to be applied to the transition currents. Different choices are possible, leading to different versions of the $1/N_c$ expansion.

The present study considers three kinematic regimes (see Table I for a summary):

(I) Low-energy elastic regime: This is the regime of scattering energies below the physical Δ threshold, $m_N < \sqrt{s} < m_\Delta$. The $1/N_c$ scaling of the scattering energy and c.m. momentum in this regime are $\sqrt{s} - m_N = \mathcal{O}(N_c^{-1})$ and $k = \mathcal{O}(N_c^{-1})$. This regime therefore has a vanishing extent $\mathcal{O}(N_c^{-1})$ in the large-N_c limit. In this regime the only open channel in the intermediate and final states is the nucleon. Both in this regime (and the following inelastic regime II) the electric term in the current and the isovector magnetic one become of the same order. As seen later, in those regimes, the effect of terms in the

TABLE I. Kinematic regimes in application of the $1/N_c$ expansion to low-energy electron scattering.

	Energy regime	$1/N_c$ expansion regime	Channels open	Final states possible
I	$m_N < \sqrt{s} < m_\Delta$	$\sqrt{s} - m_N \sim N_c^{-1}$, $k \sim N_c^{-1}$	N	Elastic
II	$m_\Delta < \sqrt{s} \ll m_{N*}$	$\sqrt{s} - m_N \sim N_c^{-1}$, $k \sim N_c^{-1}$	N, Δ	Elastic or inelastic
III	$m_\Delta < \sqrt{s} \lesssim m_{N*}$	$\sqrt{s} - m_N \sim N_c^{0}$, $k \sim N_c^{0}$	N, Δ, N^*(suppr)	Elastic or inelastic

asymmetry involving the electric charge become very important for the proton.

(II) Low-energy inelastic regime: This is the regime of scattering energies above the physical Δ threshold but significantly below the N^* threshold, $m_\Delta < \sqrt{s} \ll m_{N*}$. The $1/N_c$ scaling of the scattering energy and c.m. momentum in this regime are $\sqrt{s} - m_N = \mathcal{O}(N_c^{-1})$ and $k = \mathcal{O}(N_c^{-1})$ (same as I), but the Δ channel is now open. This regime can be treated within the low-energy expansion, in which the momenta are counted as $\mathcal{O}(N_c^{-1})$ [34,39]. Because the momentum transfer at the vertices is parametrically small, $t = \mathcal{O}(N_c^{-1})$, the t dependence of the form factors is formally suppressed. In reality one observes significant numerical effects from the momentum dependence of the form factors already in this regime (see Sec. IV).

(III) Intermediate-energy inelastic regime: This is the regime where the scattering energy is above the Δ threshold and can reach values up to and including the first resonance region, $m_\Delta < \sqrt{s} \lesssim m_{N*}$. The $1/N_c$ scaling of the scattering energy and c.m. momentum are now $\sqrt{s} - m_N = \mathcal{O}(N_c^0)$ and $k = \mathcal{O}(N_c^0)$, parametrically larger than in I and II. Both Δ and N^* states are now accessible as intermediate states (the amplitude for $N \to N^*$ transitions are suppressed compared to $N \to N, \Delta$ transitions by $N_c^{-1/2}$ [40,41]). This regime corresponds to the conventional $1/N_c$ expansion of baryon form factors at momentum transfers $t = \mathcal{O}(N_c^0)$ and was considered in Ref. [42]. The t dependence of the baryon form factors plays an essential role in this regime.

Besides the baryon resonances, also nonresonant πN states can contribute to the TSSA in inclusive eN scattering as intermediate and final states. The importance of these contributions can be rigorously assessed in the three regimes I–III. In the low-energy regimes I and II, one can perform a combined chiral and $1/N_c$ expansion using the ξ power counting scheme [34,39], where k and $1/N_c$ are counted as $\mathcal{O}(\xi)$. The pion-baryon coupling is given by $\frac{6g_A}{5F_\pi} k_\pi^i \hat{G}^{ia}$, where $g_A = \mathcal{O}(N_c)$ is the nucleon isovector axial coupling, k_π is the pion momentum, and a is the pion isospin. The three body phase space brings in a generic suppression factor $k^2/(32\pi^2)$. With these ingredients, and using the spin-flavor algebra, one finds that in the low-energy regimes I and II the contribution of nonresonant πN states to the eN cross section is suppressed by at least $\mathcal{O}(\xi^2)$ with respect to the leading order of the present calculation, and thus it is consistent to neglect it. In the intermediate-energy regime III, where the pion momenta are $\mathcal{O}(N_c^0)$ and not small, the suppression is no longer as effective, and nonresonant πN states can contribute at subleading order of the calculation performed in this work. If one limits oneself to the final states N and Δ as in this work, then the calculation only misses the πN continuum in the box diagram, and those are only affecting subleading contributions in regime III.

The numerical boundaries of these regimes in the eN c.m. momentum k, Eq. (8), are as follows: The Δ threshold $\sqrt{s} = m_\Delta = 1.23$ GeV is at $k = 0.26$ GeV; the generic N^* threshold $\sqrt{s} = m_{N*} \approx 1.5$ GeV is at $k \approx 0.46$ GeV. The expansion scheme of regime II should be applicable for $0.26 < k \lesssim 0.35$ GeV; that of regime III for $0.3 \lesssim k \lesssim 0.6$ GeV [42]. The quality of the approximation at upper end of the c.m. momentum ranges depends on the size of N^* contributions, which cannot be estimated with the present method.

The kinematic regimes introduced here provide additional justification for setting the contribution of the neutron electric form factor to zero, $G_E^n \equiv 0$, on the following basis: G_E^n vanishes at $t = 0$ and attains its maximum value at $-t \sim 0.35$ GeV^2, where it is less than 10% the value of G_E^p. In the low-energy regimes I and II, where $t = \mathcal{O}(N_c^{-2})$, G_E^n can be expanded around $t = 0$ as $G_E^n(t) = G_E^{n\prime} t$, with $G_E^{n\prime} = \mathcal{O}(N_c^0)$, and its overall contribution is $\mathcal{O}(N_c^{-2})$, beyond the accuracy of the present calculation. In the intermediate-energy regime III, the asymmetry is dominated by the large magnetic form factors $\mathcal{O}(N_c)$, and the contribution of $G_E^n(t)$ is parametrically subleading and numerically negligible. Thus, in all regimes considered in the present study, the contributions from G_E^n can be neglected.

B. Amplitude and cross section

The scattering amplitude for the process $eN \to e'B(B = N, \Delta)$ in the c.m. frame of the eN collision (see Fig. 1) is denoted by

$$M(\boldsymbol{k}_\mathrm{f}, \boldsymbol{k}_\mathrm{i} | \lambda; S_\mathrm{f} S_{\mathrm{f}3} I_{\mathrm{f}3}; S_\mathrm{i} S_{\mathrm{i}3} I_{\mathrm{i}3}). \tag{15}$$

Here λ is the electron helicity—the spin projection on $\boldsymbol{k}_\mathrm{i}$ in the initial state and $\boldsymbol{k}_\mathrm{f}$ in the final state, which is conserved in the scattering process (the electron mass is neglected). $S_\mathrm{i} S_{\mathrm{i}3} I_{\mathrm{i}3}$ are the spin-isospin quantum numbers of the initial

nucleon state, where $S_i = \frac{1}{2}$ and $I_{i3} = \pm\frac{1}{2}$ for proton/neutron. $S_f S_{f3} I_{f3}$ are the quantum numbers of the final baryon state, with $S_f = \frac{1}{2}$ or $\frac{3}{2}$ for N or Δ, and $I_{f3} = I_{i3}$. The spins of the initial and final baryons are quantized along a common axis, which can be chosen, e.g., as the direction of the initial momenta in the c.m. frame. The differential cross section for the scattering of unpolarized electrons on polarized nucleons, Eq. (4), is obtained as[3]

$$\frac{d\sigma}{d\Omega} = \frac{|\boldsymbol{k}_f|}{64\pi^2 |\boldsymbol{k}_i| s} \sum_{S_f S_{f3}} \sum_{\bar{S}_{i3} S_{i3}} \rho(S_{i3}\bar{S}_{i3}) \frac{1}{2} \sum_{\lambda} \times M^*(\boldsymbol{k}_f, \boldsymbol{k}_i|\lambda; S_f S_{f3}; S_i \bar{S}_{i3})\, M(\boldsymbol{k}_f, \boldsymbol{k}_i|\lambda; S_f S_{f3}; S_i S_{i3}). \tag{16}$$

The initial nucleon spin projection is averaged over with the spin density matrix

$$\rho(S_{i3}\bar{S}_{i3}) = \frac{1}{2}[\delta(S_{i3}\bar{S}_{i3}) + \boldsymbol{a}\cdot\boldsymbol{\sigma}(S_{i3}\bar{S}_{i3})], \tag{17}$$

where $\boldsymbol{a}$ is nucleon spin three-vector in Eq. (4) in the c.m. frame and $\boldsymbol{\sigma}$ are the Pauli matrices. The unpolarized cross section is given by the diagonal sum over initial nucleon spins. The polarized cross section for polarization normal to the scattering plane $\boldsymbol{a} = \boldsymbol{e}^y$ is given by the nondiagonal sum over nucleon spins with the matrix σ^y.

Equation (16) includes the summation over the final baryon spin $S_f = \frac{1}{2}, \frac{3}{2}$ (N, Δ) and represents the cross section for inclusive scattering. In the following also the individual contributions of N and Δ final states will be computed and quoted.

C. Spin-independent cross section

The eN scattering amplitude is computed as an expansion in the EM coupling,

$$M(\boldsymbol{k}_f, \boldsymbol{k}_i|\lambda; S_f S_{f3}; S_i S_{i3}) \equiv M_{fi} = M_{fi}^{(e2)} + M_{fi}^{(e4)} + \cdots. \tag{18}$$

The e^2 term is the standard OPE amplitude. It is given by the contraction of the electron and baryon current with the photon propagator,

$$M_{fi}^{(e2)} = -\frac{e^2}{q^2} \bar{u}(k_f)\gamma_\mu u(k_i)\, \langle B_f|J^\mu_{EM}(q)|B_i\rangle, \tag{19}$$

[3]The amplitude Eq. (15) and the cross section Eq. (16) use the relativistic normalization convention for the electron and baryon momentum states, $\langle p'|p\rangle = 2p^0(2\pi)^3\delta^{(3)}(\boldsymbol{p}'-\boldsymbol{p})$. Reference [42] used the nonrelativistic normalization $\langle p'|p\rangle = (2\pi)^3\delta^{(3)}(\boldsymbol{p}'-\boldsymbol{p})$ for the baryon states. The relativistic convention used here is more transparent for keeping track of kinematic effects caused by the N–Δ mass difference, which appear in higher orders of the $1/N_c$ expansion.

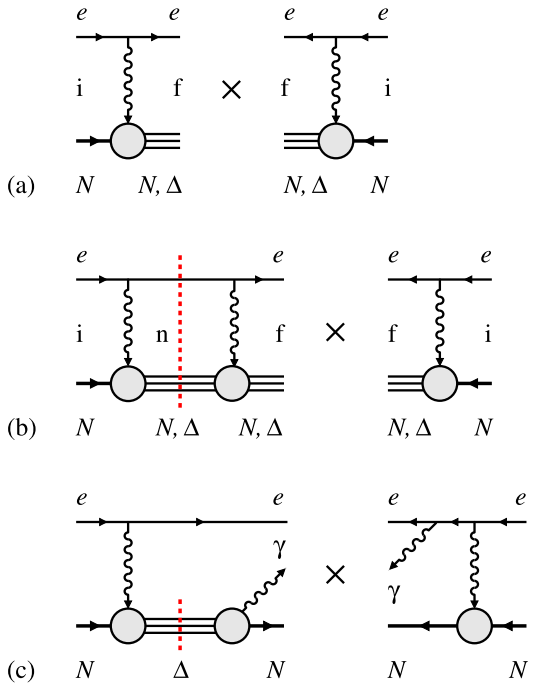

FIG. 2. Inclusive electron-nucleon scattering cross section with N and Δ final states in the $1/N_c$ expansion in the kinematic regimes described in Sec. III A. (a) Spin-independent cross section from square of e^2 amplitudes. The circle denotes the electromagnetic current matrix element between baryon states. (b) Spin-dependent cross section from interference of e^4 and e^2 amplitudes. (c) Interference of real photon emission from electron and baryon (not included in this work).

where $B \equiv \{SS_3I_3\}$ collectively denotes the baryon spin-flavor quantum numbers. The squared modulus of this amplitude gives the OPE cross section [see Fig. 2(a)], which is independent of the target spin. The explicit form of the OPE cross section generated by the $1/N_c$-expanded baryon currents, Eqs. (9) and (10), can be obtained from Eqs. (16) and (19) using standard techniques. The result is summarized in Appendix C, Eq. (C1), for the case of elastic scattering (final N, $S_f = \frac{1}{2}$).

For the purpose of the present study the spin-independent cross section is needed only as the denominator of the TSSA Eq. (7) and can be taken at the lowest order in EM coupling, i.e., as the OPE cross section. For simplicity in the following the asymmetry will be computed with the elastic rather than the inclusive OPE cross section in the denominator; this choice facilitates the discussion of the behavior near the Δ threshold.

D. Spin-dependent cross section from two-photon exchange

The spin-dependent cross section for unpolarized electron scattering is zero at the OPE order because the amplitude is real (Christ-Lee theorem) [43]. The first nonzero contribution appears through the interference

between the OPE amplitude and the imaginary (absorptive) part of the TPE amplitude, which is given by the order e^4 box diagram [see Fig. 2(b)]. The imaginary part arises from the TPE process with physical (on-shell) intermediate states, and can be computed by taking the product of the OPE amplitudes of order e^2 and integrating over the phase space of the intermediate states.

Explicitly, the e^4 amplitude resulting from the box diagram is given by

$$M_{\rm fi}^{(e4)}(S_{\rm n}) = -ie^4 \int \frac{d^4k_{\rm n}}{(2\pi)^4} \frac{1}{((k_{\rm i}-k_{\rm n})^2+i\epsilon)((k_{\rm n}-k_{\rm f})^2+i\epsilon)} \bar{u}(k_{\rm f})\gamma_\nu \frac{1}{\not{k}_{\rm n}-m_e+i\epsilon}\gamma_\mu u(k_{\rm i}) \times \sum_{S_{3n}I_{3n}} \langle B_{\rm f}|J^\nu_{\rm EM}(k_{\rm n}-k_{\rm f})|B_{\rm n}\rangle \frac{2m_{B_{\rm n}}}{(p_{\rm i}+k_{\rm i}-k_{\rm n})^2-m^2_{B_{\rm n}}+i\epsilon} \langle B_{\rm n}|J^\mu_{\rm EM}(k_{\rm i}-k_{\rm n})|B_{\rm i}\rangle, \tag{20}$$

where k_n is the 4-momentum of the electron in the intermediate state. The amplitude is presented for a given spin of the baryon B_n in the intermediate state, $S_{\rm n}$; the spin/isospin projections $S_{3\rm n}$ and $I_{3\rm n}$ are summed over. In the present case, where the initial baryon is a nucleon, $S_{\rm i}=\frac{1}{2}$, the intermediate baryons can only be N or Δ, $S_{\rm n}=\frac{1}{2}$ or $\frac{3}{2}$. The absorptive part of the amplitude is obtained by applying the Cutkosky rules. The interference of the e^2 and e^4 amplitudes needed for the spin-dependent cross section then becomes

$$M_{\rm fi}^{(e2)^*} M_{\rm fi}^{(e4)}(S_{\rm n})|_{\rm abs} + {\rm c.c.} = \frac{e^6 m_{B_{\rm n}}}{32\pi^2 t\sqrt{s}|\boldsymbol{k}_{\rm i}||\boldsymbol{k}_{\rm f}||\boldsymbol{k}_{\rm n}|} {\rm Im}\left(\int d\Omega_{\boldsymbol{k}_{\rm n}} \frac{L_{\mu\nu\rho}(k_{\rm i},k_{\rm f},k_{\rm n}) H^{\mu\nu\rho}_{\rm fi,n}(k_{\rm i},k_{\rm f},k_{\rm n})}{(1-\hat{\boldsymbol{k}}_{\rm i}\cdot\hat{\boldsymbol{k}}_{\rm n})(1-\hat{\boldsymbol{k}}_{\rm f}\cdot\hat{\boldsymbol{k}}_{\rm n})}\right). \tag{21}$$

Here the momenta are in the c.m. frame. $\hat{\boldsymbol{k}}_{\rm i}, \hat{\boldsymbol{k}}_{\rm f}$, and $\hat{\boldsymbol{k}}_{\rm n}$ are the unit vectors along the initial, final, and intermediate electron momenta; the moduli $|\boldsymbol{k}_{\rm i}|$ and $|\boldsymbol{k}_{\rm i}|$ are given by Eq. (8), and $|\boldsymbol{k}_{\rm n}|$ is given by the same expression with the intermediate baryon mass $m_{B_{\rm n}}$. The spin-dependent cross section resulting from TPE is then given by

$$e^\mu_N a_\mu \frac{d\sigma_N}{d\Omega}(I_{3\rm i}, S_{\rm f}, S_{\rm n}) = \frac{\alpha^3}{16\pi}\frac{|\boldsymbol{k}_{\rm f}|}{|\boldsymbol{k}_{\rm i}|}\frac{m_N m_{B_{\rm f}} m_{B_{\rm n}}}{ts^{3/2}|\boldsymbol{k}_{\rm i}||\boldsymbol{k}_{\rm f}||\boldsymbol{k}_{\rm n}|} {\rm Im}\left(\int d\Omega_{\hat{\boldsymbol{k}}_{\rm n}} \frac{L_{\mu\nu\rho}(k_{\rm i},k_{\rm f},k_{\rm n}) H^{\mu\nu\rho}_{\rm fi,n}(k_{\rm i},k_{\rm f},k_{\rm n})}{(1-\hat{\boldsymbol{k}}_{\rm i}\cdot\hat{\boldsymbol{k}}_{\rm n})(1-\hat{\boldsymbol{k}}_{\rm f}\cdot\hat{\boldsymbol{k}}_{\rm n})}\right). \tag{22}$$

The leptonic and hadronic tensors in the above expressions are given by

$$\begin{aligned} L^{\mu\nu\rho}(k_{\rm i},k_{\rm f},k_{\rm n}) &= {\rm Tr}(\not{k}_{\rm i}\gamma^\mu \not{k}_{\rm f}\gamma^\nu \not{k}_{\rm n}\gamma^\rho), \\ &= 4(k_{\rm i}^\mu k_{\rm n}^\rho k_{\rm f}^\nu + k_{\rm i}^\mu k_{\rm n}^\nu k_{\rm f}^\rho + k_{\rm i}^\rho (k_{\rm n}^\nu k_{\rm f}^\mu + k_{\rm n}^\mu k_{\rm f}^\nu - k_{\rm n}\cdot k_{\rm f} g^{\mu\nu}) + k_{\rm i}^\nu (k_{\rm n}^\rho k_{\rm f}^\mu - k_{\rm n}^\mu k_{\rm f}^\rho + k_{\rm n}\cdot k_{\rm f} g^{\mu\rho}) \\ &\quad - (k_{\rm i}^\mu k_{\rm n}\cdot k_{\rm f} - k_{\rm i}\cdot k_{\rm f} k_{\rm n}^\mu + k_{\rm i}\cdot k_{\rm n} k_{\rm f}^\mu) g^{\nu\rho} - k_{\rm i}\cdot k_{\rm f} k_{\rm n}^\rho g^{\mu\nu} - k_{\rm i}\cdot k_{\rm f} k_{\rm n}^\nu g^{\mu\rho} - k_{\rm i}\cdot k_{\rm n} k_{\rm f}^\nu g^{\mu\rho} + k_{\rm i}\cdot k_{\rm n} k_{\rm f}^\rho g^{\mu\nu}), \end{aligned} \tag{23}$$

$$H^{\mu\nu\rho}_{\rm fi,n}(k_{\rm i},k_{\rm f},k_{\rm n}) = \sum_{\bar{S}_{\rm i3}S_{\rm i3}} \frac{1}{2}\boldsymbol{a}\cdot\boldsymbol{\sigma}(S_{\rm i3}\bar{S}_{\rm i3}) \sum_{S_{\rm f3}I_{\rm f3}} \sum_{S_{\rm n3}I_{\rm n3}} \langle B_{\rm i}|(J^\mu_{\rm EM}(k_{\rm i}-k_{\rm f}))^\dagger|B_{\rm f}\rangle \langle B_{\rm f}|J^\nu_{\rm EM}(k_{\rm n}-k_{\rm f})|B_{\rm n}\rangle \langle B_{\rm n}|J^\rho_{\rm EM}(k_{\rm i}-k_{\rm n})|B_{\rm i}\rangle. \tag{24}$$

Equation (22) presents the cross section depending on the isospin projection of the initial nucleon $I_{\rm i3}=\pm\frac{1}{2}$, the spin of the final baryon $S_{\rm n}=\frac{1}{2},\frac{3}{2}$; and the spin of the intermediate baryon in the box diagram $S_{\rm n}=\frac{1}{2},\frac{3}{2}$; the contributions of the different final and intermediate states will be discussed below.

The $1/N_c$ expansion is now implemented for the hadronic tensor. The method makes use of the t-channel spin and isospin of the tensor, J and I, which can be viewed as the quantum numbers of an operator connecting the nucleon states. In the spin-dependent cross section, only the $J=1$ component of the tensor is needed, and because it is a forward matrix element between the initial nucleon state and its conjugate, only the total $I=0$ or 1 components of the tensor can contribute. Thus, in the end those components of the hadronic tensor will reduce to the operators $\hat{S}^i$ and $\hat{S}^i\hat{I}^3$. The spin-flavor reduction of the hadronic tensor can be carried out for general N_c making use of the $SU(4)$ algebra. The sketch of the calculation is as follows: starting with the general structure of the product of currents

$$(J^{\mu}_{\mathrm{EM}}(k_{\mathrm{i}}-k_{\mathrm{f}}))^{\dagger}|B_{\mathrm{f}}\rangle\langle B_{\mathrm{f}}|J^{\nu}_{\mathrm{EM}}(k_{\mathrm{n}}-k_{\mathrm{f}})|B_{\mathrm{n}}\rangle\langle B_{\mathrm{n}}|J^{\rho}_{\mathrm{EM}}(k_{\mathrm{i}}-k_{\mathrm{n}}), \tag{25}$$

the spatial and the time components of the currents, as well as the isoscalar and the isovector components need separate consideration along with the projections onto the final and the intermediate baryon states. The product of currents is decomposed in two steps, namely the currents in the box diagram are first coupled to the t-channel (J_1, I_1), and then the result is coupled to the (conjugate) current of the one-photon exchange to total $(J = 1, I = 0, 1)$ as needed here. At each stage the resulting composite spin-flavor operators are decomposed into the basis of spin-flavor operators. An advantage of this procedure is that one obtains explicitly the results for generic N_c, making possible a detailed organization in powers of $1/N_c$ of the different combinations of the EM current components, with even more details such as the individual contributions of the different (J_1, I_1) and (J, I) projections.

The integrals over the intermediate momentum direction $\hat{\boldsymbol{k}}_{\mathrm{n}}$ in Eq. (21) are reduced to cases where the numerator is a tensor product of $\hat{\boldsymbol{k}}_{\mathrm{n}}$ multiplied by powers of $\hat{\boldsymbol{k}}_{\mathrm{i}} \cdot \hat{\boldsymbol{k}}_{\mathrm{n}}$ and $\hat{\boldsymbol{k}}_{\mathrm{f}} \cdot \hat{\boldsymbol{k}}_{\mathrm{n}}$ (see Appendix B). As explained in Sec. II B, the momentum dependence of the form factors needs to be included in the integral, and a common dipole form is chosen for the form factors of all components of the EM current. The integrations with these form factors are performed analytically in Appendix B.

In general, the individual integrals show IR or collinear divergencies resulting from one of the photons in the box diagram becoming soft or real within the integration domain. The collinear singularities occur for a photon coupling to a current making a transition between N and Δ, where a real photon with energy equal to the mass difference is possible, the other cases are IR singularities. Those divergencies are regulated by including an infinitesimal photon mass whose effect is represented by the parameter $\epsilon = 0^{+}$ in Appendix B. The end result is, for both cases with and without the inclusion of form factors,[4] that those divergencies of the individual contributions cancel in the imaginary part of the spin-dependent part of the integral in Eq. (22). It is important to emphasize that the cancellations of the divergencies only occur for the precise on-shell kinematics. The divergencies cancel individually for the different final and intermediate baryon states, and for each possible t-channel $(J = 1, I = 0, 1)$ and (J_1, I_1) projection of the box diagram, as far as in the TPE absorptive amplitude EM gauge invariant combinations of the two hadronic currents are considered, i.e., for terms with two different components of the EM current the two possible orderings must be added up. In particular, those cancellations serve as one useful check of the calculations.

The explicit calculation shows that for a stable Δ the interference differential cross section has a finite discontinuity at the Δ threshold. This discontinuity is only present in the elastic asymmetry, i.e., nucleon final state. It is explained as follows: the leptonic tensor is proportional to the energy E_{n} of the electron in the box, the absorptive part of the diagram has a phase space proportional to E_{n}, and each photon propagator gives a factor $1/E_{\mathrm{n}}$, so that there is a finite contribution in the limit $E_{\mathrm{n}} \to 0$, which is at the threshold for the Δ. This finite threshold enhancement is thus understood as the two photons becoming real and collinear with $\boldsymbol{k}_{\mathrm{i}}$ and $\boldsymbol{k}_{\mathrm{f}}$.

Although the Δ width is $\mathcal{O}(N_c^{-2})$, it is then necessary to include it to reproduce the realistic behavior at the onset of its contribution, resulting in a smoothing of the mentioned discontinuity. In the present calculation the width is implemented by a Breit-Wigner form, as shown in Appendix E. The effect of the width is reduced to a smearing of the Δ mass in the calculation at zero width using Eq. (E2).

IV. RESULTS

A. Evaluation and validation

The TSSA is now evaluated numerically, using the expressions obtained from the $1/N_c$ expansion of the hadronic tensor. The results cover the parametric regions I–III identified in Sec. III A and are accurate to subleading order in $1/N_c$. In regions I and II the present results are new and predict the behavior of the TSSA below and above the Δ threshold. In region III the present results can be matched with the leading-order (LO) $1/N_c$ expansion results of the previous publication [42] but include also the subleading $1/N_c$ corrections, which improve the predictions and illustrate the theoretical uncertainty.

The results shown here have been validated with two independent tests: (i) Comparison with the leading-order $1/N_c$ expansion results [42], which were evaluated using an independent algebraic method. (ii) Comparison of the nucleon-only contribution (i.e., nucleon in intermediate and final state) with the well-known result of the relativistic Feynman diagram calculation, expanded such as to match the $1/N_c$ expansion calculation.

B. Role of form factors and electric/magnetic currents

It is instructive to first display the results when the t-dependence of the form factors is neglected, as this gives a rough idea of the role of the different components of the EM current, and also serves as a reference point for the calculation with form factors. As indicated earlier, the TSSA A_N is defined in the following with respect to the unpolarized elastic cross section Eq. (C1). The results for the separate contributions to the interference term of the cross section $d\sigma_N$ by the nucleon and Δ in the intermediate

[4]The IR and collinear divergencies of individual integrals do depend on the form factors, thus additional cancellations occur in this case.

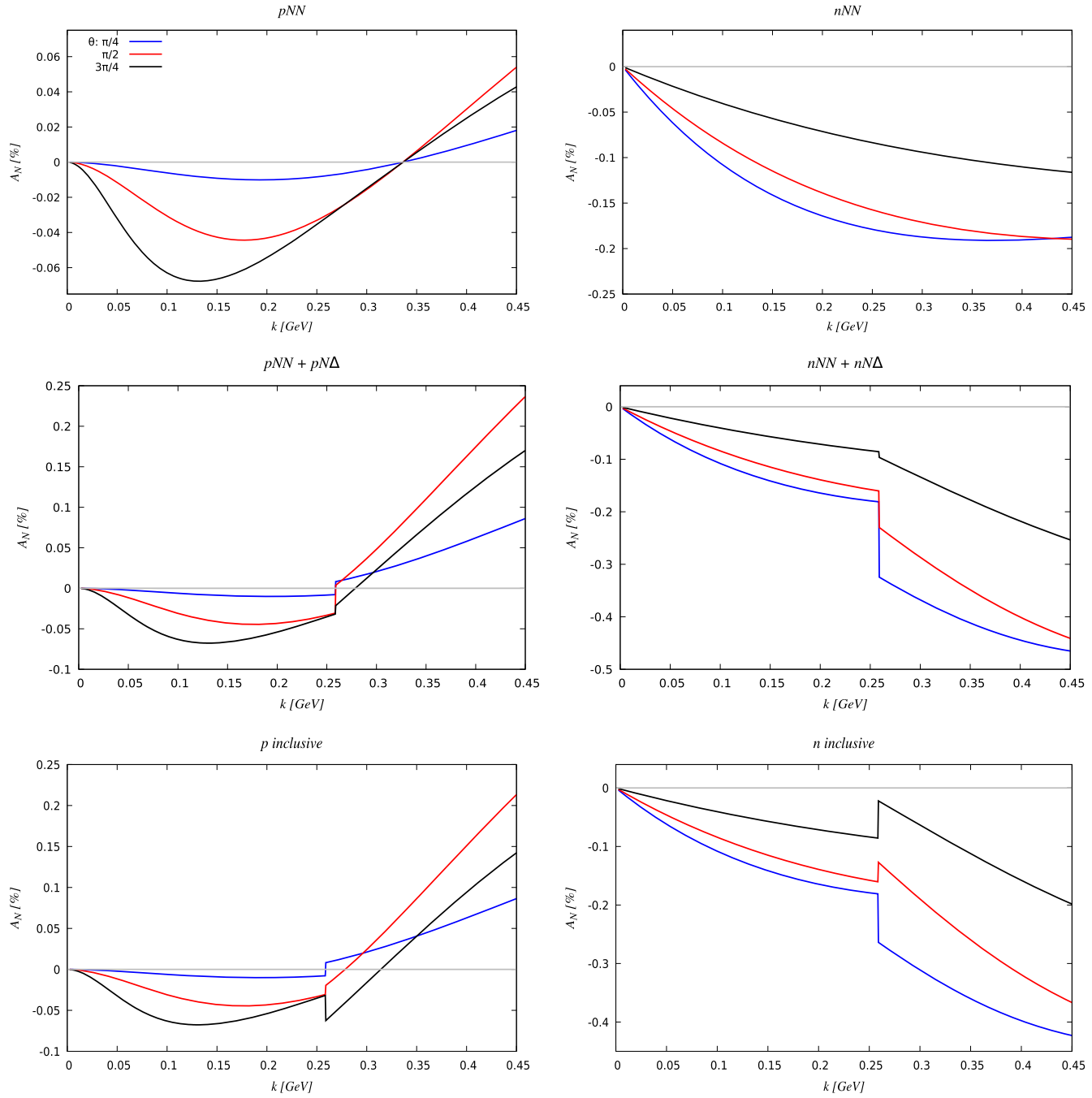

FIG. 3. A_N vs k with no form factors and stable Δ. Left/right column: proton/neutron target. Top row: elastic A_N with only nucleon in the TPE amplitude. Middle row: elastic A_N with nucleon and Δ in TPE amplitude. Bottom row: inclusive A_N.

and final states are given in Appendix D Eq. (D1). The contributions are at most linear in the electric form factors,[5] and in the strict nonrelativistic limit, independent of the nucleon mass, as one would expect. As discussed earlier, neglecting the width of the Δ leads to a finite discontinuity in the interference differential cross section in the case of a final nucleon at the Δ threshold.

Figure 3 shows the TSSA A_N evaluated without form factors (here and in the following $k \equiv |\boldsymbol{k}_i|$). It is observed that the Δ intermediate state in the box amplitude makes a large contribution to the elastic asymmetry. On the other hand, the Δ final state makes a very small contribution to

[5]A nonrelativistic expansion of the cross section starting with the relativistic one gives terms that are proportional to $(G_E/m_N)^2$; such terms are of higher order in $1/N_c$ and are not captured by the present expansion. They involve the contributions from the spatial components of the convection EM current, which to the order of the present calculation are irrelevant.

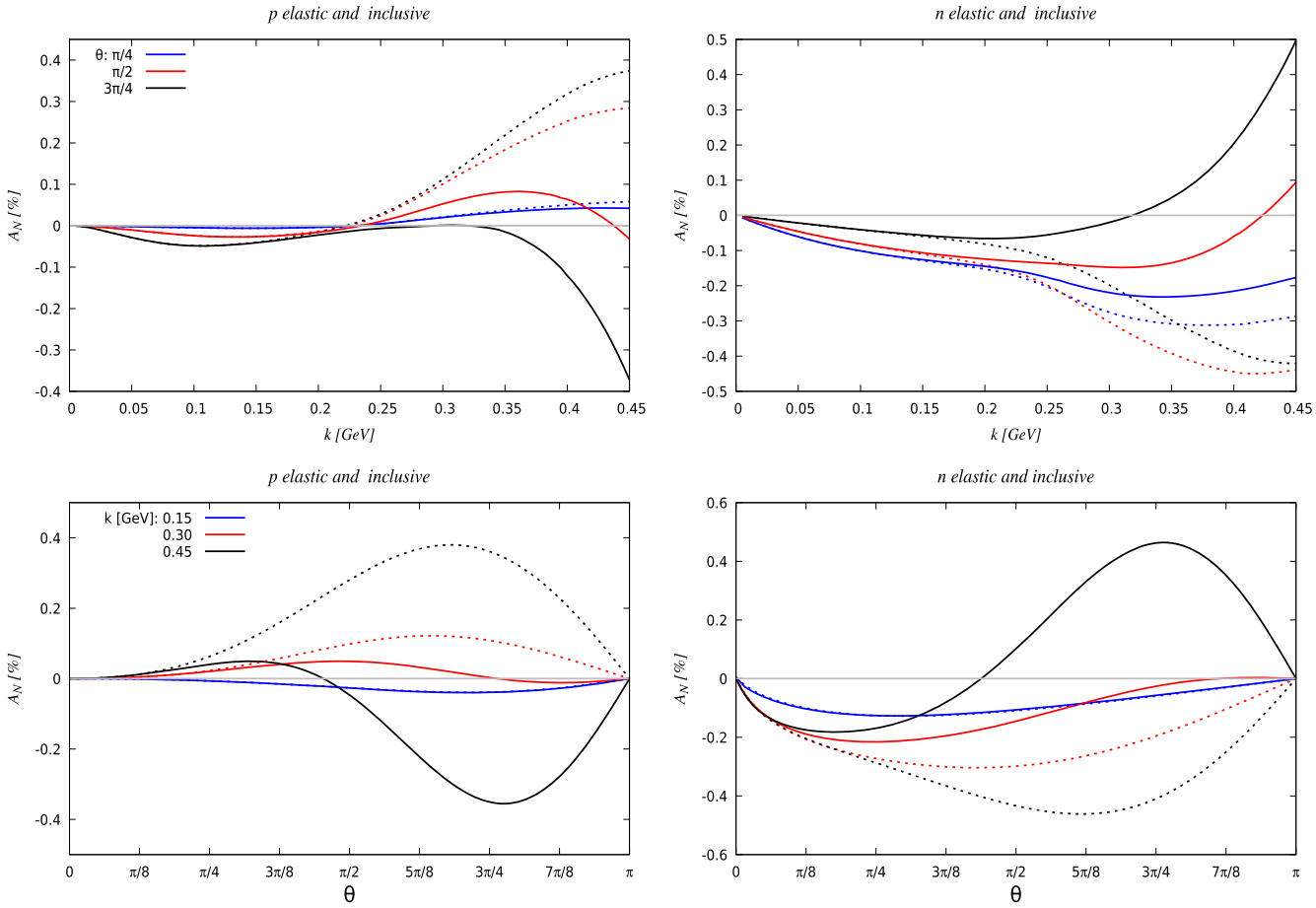

FIG. 4. A_N vs k (top row) and A_N vs θ (bottom row) with inclusion of form factors and Δ width. Proton target (left column) and neutron target (right column). Elastic (dashed lines) and inclusive (solid lines).

the inclusive asymmetry. This was observed already in the leading-order $1/N_c$ expansion in the kinematic region III in Ref. [42]. As shown below, the inclusion of the t dependence in the form factors profoundly affects the suppression of the Δ state in the inelastic asymmetry. For the proton the behavior of the asymmetry is very much affected in the kinematic domains I and II by the terms proportional to G_E, which are of opposite sign to the purely magnetic ones and larger, leading to the crossover to negative values shown in Fig. 3.

Figure 4 shows the results obtained with inclusion of the form factors and the Δ width (these represent the final numerical results and will be discussed further below). The width is implemented using $\Gamma_\Delta = 0.125$ GeV and $Q = 0.2$ GeV. Comparing with Fig. 3 one observes that the form factors have only a moderate effect on the elastic asymmetries (dashed curves in Fig. 4). However, they have a dramatic effect on the inelastic asymmetry (Δ final state). This is further illustrated by Figs. 5 and 6, which directly compare the results with and without form factors for the inelastic and inclusive (elastic + inelastic) asymmetries. In fact, for energies above the Δ threshold, the inelastic asymmetry has opposite sign to that of the elastic one and becomes increasingly dominant with energy. This effect of the form factors was observed in the leading-order $1/N_c$ expansion [42].

There is no simple argument explaining the effects of the form factors in the absorptive part of the box diagram observed here. However, some insight can be gained from considering the large-N_c limit, where the leading-order $1/N_c$ expansion result becomes exact. One finds that logarithmic terms $\propto \log \sin^2 \frac{\theta}{2}$ are important in the interference cross section for elastic and inelastic final states. In the inelastic case there is a strong cancellation between these logarithmic terms and polynomial terms in $\sin^2 \frac{\theta}{2}$ when the form factors are neglected, giving the small inelastic interference cross section. This cancellation is upset when the form factors are included, resulting in the strong sensitivity of the inelastic TSSA to the form factors. In the strict large N_c limit, the contribution to the elastic asymmetry by the Δ intermediate state in the box is twice that of the N. In the physical case, with the subleading terms in the EM current included, one finds a similar result for the case of the neutron, while the contribution of the Δ

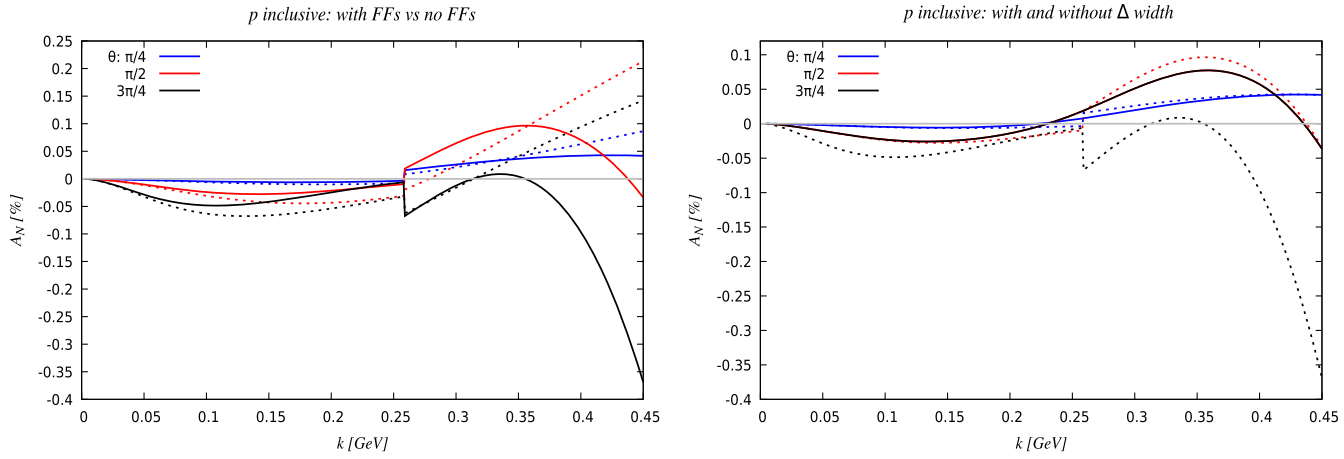

FIG. 5. Inclusive A_N for proton target. Left panel: comparison of results without form factors (dashed lines) and with form factors (solid lines). Right panel: comparison of results without Δ width (dashed) and with Δ width (solid); both are with form factors.

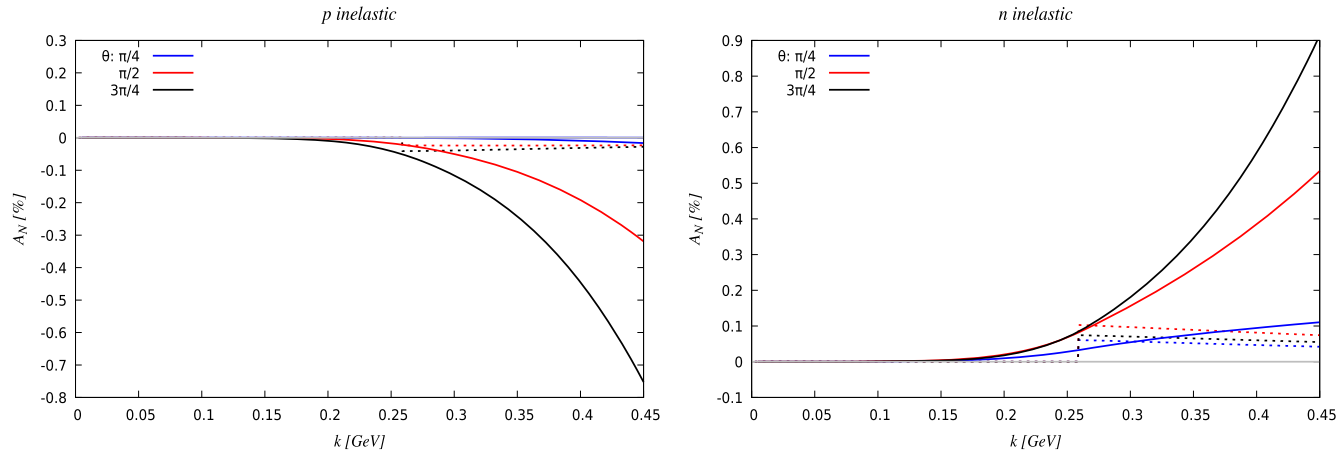

FIG. 6. Inelastic A_N for proton (left panel) and neutron target (right panel). Comparison between results without form factors (dashed lines) and with form factors (solid lines).

is further enhanced for the proton. On the other hand, for Δ in the final state, in the strict large N_c limit, the contribution of the N in the box is five times as large as that of the Δ. This remains roughly the same in the physical case for both proton and neutron.

C. Size of $1/N_c$ corrections

It is interesting to investigate the size of $1/N_c$ corrections in the TSSA. This serves to illustrate the convergence of the parametric expansion and quantify the numerical uncertainty.

The LO $1/N_c$ expansion in kinematic region III, $k = \mathcal{O}(N_c^0)$, was considered in Ref. [42]. In this order the N and Δ are degenerate, and only the isovector magnetic component of the EM current contributes. The LO contributions to the TSSA are $\mathcal{O}(\alpha N_c)$ and arise from the hadronic currents in the box being coupled to $I_1 = J_1$, which can only be $I_1 = J_1 = 0$ if the final state is N (elastic) and $I_1 = J_1 = 2$ if the final state is Δ (inelastic). Using the results of the present calculation, it is now possible to compute the $1/N_c$ corrections in region III. They arise from the LO components of the two currents in the box diagram coupled to $I_1 \neq J_1$, and from the subleading components of the EM current. At this order also the mass difference $m_\Delta - m_N$ must be included. Furthermore, it is possible to compute the size of $1/N_c$ corrections in regions I and II, $k = \mathcal{O}(N_c^{-1})$, which is also covered by the present expressions.

Figure 7 shows the comparison of the LO and NLO results. Here the correct phase space, with the finite N–Δ mass splitting, is used for the LO result. For the neutron one sees that the LO result is close to the NLO one, which is easy to understand as the contributions are purely magnetic, and the only difference is the disregard of the isoscalar magnetic term at LO. On the other hand, for the proton the effect of the electric term in the current, which is not present

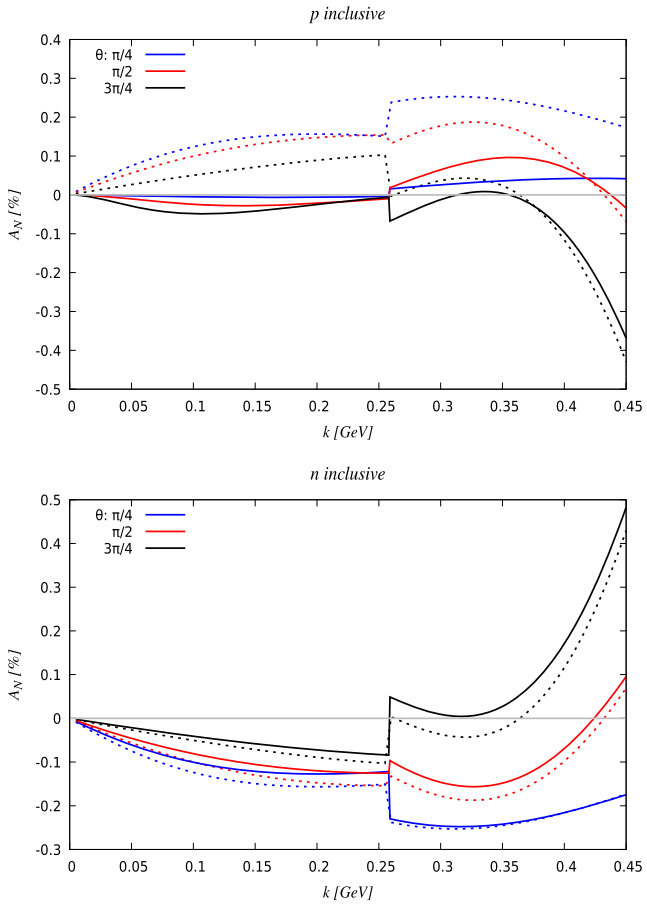

FIG. 7. Inclusive A_N for proton (left panel) and neutron target (right panel). Comparison between the LO in $1/N_c$ (dashed lines) and the results of this work (solid lines). Form factors are included, and the physical phase space is used in the LO result.

at LO, leads to a big difference at NLO. As mentioned earlier, the modified power counting implied in the kinematic regions I and II shows the relevance of the electric contributions, especially at the smaller angles. At larger energies and scattering angle the purely magnetic contributions become dominant, and the LO approximation is remarkably good (black curve in Fig. 7).

D. Final results

The results of Fig. 4 represent the final numerical estimate of the TSSA and should be used to discuss its kinematic dependencies and potential measurements. It is worth noting the following features: (i) The elastic and inclusive asymmetries are of the order few $\times 10^{-3}$ for $k \lesssim 0.5$ GeV, for both proton and neutron. (ii) The inelastic contribution to the asymmetry above the Δ threshold has opposite sign to the elastic one, and at large angles and energy $k > 0.35$ GeV is about a factor of 2 larger in magnitude than the elastic one. (iii) As a function of the scattering angle, the elastic TSSA has its maximum magnitude at increasing angles for increasing energy, for both proton and neutron. The elastic asymmetries do not change sign, while the inclusive ones do.

V. DISCUSSION

The TSSA for electron nucleon scattering was evaluated in the energy range below the second resonance region employing a method based on he $1/N_c$ expansion. The method makes use of the dynamical constraints that the large N_c limit imposes in the baryon sector, which result in a spin-flavor approximate symmetry broken by subleading corrections that are organized in a $1/N_c$ expansion. That symmetry in particular unifies the treatment of the nucleon and Δ resonance, allowing for the systematic analysis carried out here that includes the first subleading terms in the $1/N_c$ expansion. The analysis gives results for the elastic and inelastic asymmetry, and also provides details on the separate N and Δ contributions in the absorptive part of the TPE scattering amplitude.

It is found that form factors play a crucial role, in particular in enhancing the inelastic asymmetry. The latter turns out to have, for c.m. scattering angles larger than 90°, an opposite sign to that of the elastic one and significantly larger in magnitude. For electron c.m. momenta below 0.5 GeV the TSSA is found to be in the range 10^{-3}–10^{-2}. If experiments in this energy domain could be performed, measurements of the TSSA should be feasible.

Some comments are in order regarding the accuracy of the estimates based on the $1/N_c$ expansion. At the next-to-leading-order (NLO) accuracy of the present calculation, the structures in the baryon EM currents are the charges and the magnetic moment components. The next-to-next-to-leading-order (NNLO) terms, not included in the present analysis, involve in addition the spatial component of the convection current, the electric quadrupole component, and corrections to the structures already considered which depend on the baryon spin, i.e., terms that include an extra factor $\hat{S}^2/N_c^2$ in the magnetic components of the current, which modify the LO relations between N and Δ magnetic moments. The NNLO terms neglected in the calculation are expected to have a natural size, and their relative effect can be estimated as $\sim 1/N_c^2|_{N_c=3} = 1/9$ times a coefficient of order unity. Such accuracy was observed in previous implementations of the $1/N_c$ expansion as a low-energy expansion with $k = \mathcal{O}(N_c^{-1})$ [34,39], and should naturally extend to the kinematic regime $k = \mathcal{O}(N_c^0)$ below the higher resonances.

When the energy rises above the threshold, the N^*s can appear as an intermediate state in the TPE amplitude. Generically, the transition matrix elements of the EM current from ground state baryons to higher resonances carry an additional suppression factor $1/\sqrt{N_c}$ [37,40,41]. The contribution of individual N^* resonances to the TPE amplitude are therefore suppressed by a factor $\mathcal{O}(N_c^{-1})$ relative to the leading order of the calculation in kinematic

region III; however, they might be numerically large. The inclusion of N^* intermediate states in the present calculation of the TSSA in kinematic region III would be an interesting future extension of the present study.

The transition of the TSSA to the high-energy regime will involve the cumulative contributions of many resonances, as intermediate states in the TPE amplitude and as final states in the cross section. In this situation the $\mathcal{O}(N_c^{-1})$ suppression of individual N^* contributions is no longer effective, and the accounting changes. It is expected that both the elastic and the inclusive TSSA in this regime are generated by TPE amplitudes at the quark level. Different arguments have been put forward regarding the dominance of scattering from the same quark or different quarks. The duality of the descriptions as cumulative resonance contributions and scattering from quarks is an interesting theoretical problem. Measurements of the TSSA in the resonance region could provide valuable material for further studies.

The cross section for inclusive eN scattering at $\mathcal{O}(\alpha^3)$ includes also real photon emission into the final state, $e + N \to e' + \gamma + X'$. A TSSA can appear from the interference of the amplitudes of real photon emission by the nucleon and by the electron—the so-called virtual Compton scattering and Bethe-Heitler processes [Fig. 2(c)]. It requires that the amplitude of real photon emission from the nucleon have an imaginary part [8]. In the low-energy regime considered here, this is possible if the intermediate state is a Δ. This contribution to the TSSA can be analyzed in the $1/N_c$ expansion approach in the same manner as the TPE contribution [Fig. 2(b)]. In the kinematic region III, where $k = \mathcal{O}(N_c^0)$, parametric analysis shows that the real photon emission contribution is suppressed at least by a factor $1/N_c$ compared to the TPE contribution. This happens because the energy of the emitted photon in the c.m. frame is of the order of the N–Δ mass difference $m_\Delta - m = \mathcal{O}(N_c^{-1})$; its momentum is therefore $k_\gamma = \mathcal{O}(N_c^{-1})$; and its coupling to the dominant isovector magnetic vertex is suppressed by $1/N_c$. Here the $1/N_c$ expansion reproduces the well-known result from "soft photons" physics in QED, that such photons couple only to the charge of the colliding particles but not to their spin [44]. The calculation of real photon emission in kinematic region III to leading non-vanishing order, and the extension of the above analysis to region II, remain interesting problems for future study.

TPE also gives rise to a transverse beam spin asymmetry in eN scattering. It is proportional to the electron mass and expected to be several orders of magnitude smaller than the target spin asymmetry [13,45–49]. The transverse beam spin asymmetry can be measured in electron scattering experiments with high beam polarization quality as used for parity-violating scattering; it represents an important background to the longitudinal beam spin asymmetry caused by weak interactions parity-violating electron scattering. It could also be measured in μN scattering, where it is enhanced by the muon mass [49]. The $1/N_c$ expansion method developed here can be extended to calculate the beam spin asymmetry in elastic or inclusive eN scattering in the resonance region. Work on this extension is in progress.

ACKNOWLEDGMENTS

This material is based upon work supported by the U.S. Department of Energy, Office of Science, Office of Nuclear Physics under Contract No. DE-AC05-06OR23177 (J. L. G. and C. We.), by the National Science Foundation, Grant No. PHY 1913562 (J. L. G.) and by the Fonds de la Recherche Scientifique (FNRS) (Belgium), Grant No. 4.45.10.08 (C. Wi.).

APPENDIX A: $SU(4)$ ALGEBRA

This appendix summarizes properties of the $SU(4)$ spin-flavor symmetry group used in the present analysis. The algebra of $SU(4)$ contains 15 generators: the spin generators $\hat{S}^i$, the isospin generators $\hat{I}^a$, and the spin-flavor generators $\hat{G}^{ia}$, where i and a run from 1 to 3. The commutation relations are

$$[\hat{S}^i, \hat{S}^j] = i\epsilon^{ijk}\hat{S}^k, \qquad [\hat{I}^a, \hat{I}^b] = i\epsilon^{abc}\hat{I}^c, \qquad [\hat{I}^a, \hat{S}^i] = 0,$$
$$[\hat{S}^i, \hat{G}^{ja}] = i\epsilon^{ijk}\hat{G}^{ka}, \qquad [\hat{I}^a, \hat{G}^{ib}] = i\epsilon^{abc}\hat{G}^{ic},$$
$$[\hat{G}^{ia}, \hat{G}^{jb}] = \frac{i}{4}\delta^{ij}\epsilon^{abc}\hat{I}^c + \frac{i}{4}\delta^{ab}\epsilon^{ijk}\hat{S}^k. \tag{A1}$$

The ground state baryon states fill the $SU(4)$ representation formed by totally symmetric tensors with N_c indices. These states have spin/isospin $S = I = \frac{1}{2}\cdots\frac{N_c}{2}$ and are denoted by $|SS_3I_3\rangle$. The matrix elements of the $SU(4)$ generators in these states are

$$\langle S'S'_3I'_3|\hat{S}^i|SS_3I_3\rangle = \sqrt{S(S+1)}\delta_{S'S}\delta_{I'_3I_3}\langle SS_3, 1i|S'S'_3\rangle, \tag{A2}$$

$$\langle S'S'_3I'_3|\hat{I}^a|SS_3I_3\rangle = \sqrt{S(S+1)}\delta_{S'S}\delta_{I'_3I_3}\langle SI_3, 1a|S'I'_3\rangle, \tag{A3}$$

$$\langle S'S'_3I'_3|\hat{G}^{ia}|SS_3I_3\rangle = \frac{1}{4}\sqrt{\frac{2S+1}{2S'+1}}\sqrt{(N_c+2)^2 - (S-S')^2(S+S'+1)^2} \times \langle SS_3, 1i|S'S'_3\rangle\langle SI_3, 1a|S'I'_3\rangle. \tag{A4}$$

$\hat{S}^i$ and $\hat{I}^a$ have matrix elements $\mathcal{O}(N_c^0)$ and connect only states with $S' = S$; $\hat{G}^{ia}$ have matrix elements $\mathcal{O}(N_c)$ and can connect states with $S' = S$ or $S \pm 1$.

APPENDIX B: PHASE SPACE INTEGRALS

This appendix describes the phase space integrals arising in the calculation of the absorptive part of the box diagram in Eqs. (21) and (22). Giving explicit analytic results is important because individual integrals present infrared and/or collinear divergencies due to the photon propagators in the box, which cancel in the final result. The divergencies of the individual integrals are regulated by including an infinitesimal photon mass, provided by the regulator $\epsilon = 0^+$ below.

1. Integrals without form factors

The first set of integrals is for the case where no form factors are included. In the following the unit vector $\hat{\boldsymbol{K}}$ is the integration variable [the intermediate electron direction $\hat{\boldsymbol{k}}_{\rm n}$ in Eq. (21)], and $\hat{\boldsymbol{k}}$ and $\hat{\boldsymbol{k}}'$ are external unit vectors on which the integral depends [the initial/final electron direction $\hat{\boldsymbol{k}}_{\rm f,i}$ in Eq. (21)]. The integrals with a single denominator arising in the calculation are these:

$$\begin{aligned}
J(n) &= \int d\Omega_K \frac{(\hat{\boldsymbol{k}}\cdot\hat{\boldsymbol{K}})^n}{1-\hat{\boldsymbol{k}}\cdot\hat{\boldsymbol{K}}+\epsilon},\\
&= -2\pi\left(\log\frac{\epsilon}{2} + 2\sum_{m=0}^{\frac{[n-1]}{2}}\frac{1}{2m+1}\right),\\
J^i(\hat{\boldsymbol{k}},n) &= \int d\Omega_K \frac{\hat{\boldsymbol{K}}^i(\hat{\boldsymbol{k}}\cdot\hat{\boldsymbol{K}})^n}{1-\hat{\boldsymbol{k}}\cdot\hat{\boldsymbol{K}}+\epsilon},\\
&= \hat{\boldsymbol{k}}^i J(n+1),\\
J^{ij}(\hat{\boldsymbol{k}},n) &= \int d\Omega_K \frac{\hat{\boldsymbol{K}}^i\hat{\boldsymbol{K}}^j(\hat{\boldsymbol{k}}\cdot\hat{\boldsymbol{K}})^n}{1-\hat{\boldsymbol{k}}\cdot\hat{\boldsymbol{K}}+\epsilon},\\
&= \frac{1}{2}\{\delta^{ij}[J(n)-J(n+2)]\\
&\quad +\hat{\boldsymbol{k}}^i\hat{\boldsymbol{k}}^j[3J(n+2)-J(n)]\}.
\end{aligned} \tag{B1}$$

The integrals with a double denominator are these:

$$\begin{aligned}
J(\hat{\boldsymbol{k}},\hat{\boldsymbol{k}}',n,n') &= \int d\Omega_K \frac{(\hat{\boldsymbol{k}}\cdot\hat{\boldsymbol{K}})^n(\hat{\boldsymbol{k}}'\cdot\hat{\boldsymbol{K}})^{n'}}{(1-\hat{\boldsymbol{k}}\cdot\hat{\boldsymbol{K}}+\epsilon)(1-\hat{\boldsymbol{k}}'\cdot\hat{\boldsymbol{K}}+\epsilon)},\\
J^i(\hat{\boldsymbol{k}},\hat{\boldsymbol{k}}',n,n') &= \int d\Omega_K \frac{\hat{\boldsymbol{K}}^i(\hat{\boldsymbol{k}}\cdot\hat{\boldsymbol{K}})^n(\hat{\boldsymbol{k}}'\cdot\hat{\boldsymbol{K}})^{n'}}{(1-\hat{\boldsymbol{k}}\cdot\hat{\boldsymbol{K}}+\epsilon)(1-\hat{\boldsymbol{k}}'\cdot\hat{\boldsymbol{K}}+\epsilon)},\\
J^{ij}(\hat{\boldsymbol{k}},\hat{\boldsymbol{k}}',n,n') &= \int d\Omega_K \frac{\hat{\boldsymbol{K}}^i\hat{\boldsymbol{K}}^j(\hat{\boldsymbol{k}}\cdot\hat{\boldsymbol{K}})^n(\hat{\boldsymbol{k}}'\cdot\hat{\boldsymbol{K}})^{n'}}{(1-\hat{\boldsymbol{k}}\cdot\hat{\boldsymbol{K}}+\epsilon)(1-\hat{\boldsymbol{k}}'\cdot\hat{\boldsymbol{K}}+\epsilon)}.
\end{aligned} \tag{B2}$$

The results for these integrals as needed in the present work are given in the following tables. Here $\hat{\boldsymbol{k}}\cdot\hat{\boldsymbol{k}}' = \cos\theta$, where θ is the scattering angle.

n	n'	$J(\hat{\boldsymbol{k}},\hat{\boldsymbol{k}}',n,n')$
0	0	$\frac{4\pi}{1-\cos\theta}\left(\log\,\sin^2\frac{\theta}{2} - \log\frac{\epsilon}{2}\right)$
1	0	$J(\hat{\boldsymbol{k}},\hat{\boldsymbol{k}}',0,0) - J(0)$
1	1	$J(\hat{\boldsymbol{k}},\hat{\boldsymbol{k}}',1,0) - J(1)$
2	0	$\hat{\boldsymbol{k}}^i J^i(\hat{\boldsymbol{k}},\hat{\boldsymbol{k}}',0,0) - \cos\theta J(1)$

n	n'	$J^i(\hat{\boldsymbol{k}},\hat{\boldsymbol{k}}',n,n')$
0	0	$-2\pi\frac{\hat{\boldsymbol{k}}^i+\hat{\boldsymbol{k}}'^i}{\sin^2\theta}\left[(1+\cos\theta)\log\frac{\epsilon}{2} - 2\log\,\sin^2\frac{\theta}{2}\right]$
1	0	$J^i(\hat{\boldsymbol{k}},\hat{\boldsymbol{k}}',0,0) - \hat{\boldsymbol{k}}'^i J(1)$
1	1	$J^i(\hat{\boldsymbol{k}},\hat{\boldsymbol{k}}',0,0) - (\hat{\boldsymbol{k}}^i+\hat{\boldsymbol{k}}'^i)J(1)$
2	0	$J^i(\hat{\boldsymbol{k}},\hat{\boldsymbol{k}}',1,0) - \hat{\boldsymbol{k}}^j J^{ij}(\hat{\boldsymbol{k}}',0)$

n	n'	$J^{ij}(\hat{\boldsymbol{k}},\hat{\boldsymbol{k}}',n,n')$
0	0	$\frac{2\pi}{\cos^2\frac{\theta}{2}\sin^2\theta}\Big[-\delta^{ij}\sin^2\theta\log\,\sin^2\frac{\theta}{2}$ $+2(\hat{\boldsymbol{k}}^i\hat{\boldsymbol{k}}^j+\hat{\boldsymbol{k}}'^i\hat{\boldsymbol{k}}'^j)\Big(\log\,\sin^2\frac{\theta}{2} - \cos\theta\cos^2\frac{\theta}{2}$ $-\cos^4\frac{\theta}{2}\log\frac{\epsilon}{2}\Big)$ $+2(\hat{\boldsymbol{k}}^i\hat{\boldsymbol{k}}'^j+\hat{\boldsymbol{k}}^j\hat{\boldsymbol{k}}'^i)\Big(\cos^2\frac{\theta}{2}+\sin^2\frac{\theta}{2}\log\,\sin^2\frac{\theta}{2}\Big)\Big]$
1	0	$J^{ij}(\hat{\boldsymbol{k}},\hat{\boldsymbol{k}}',0,0) - J^{ij}(\hat{\boldsymbol{k}}',0)$

(B3)

2. Integrals with form factors

The second set of integrals is for the case where form factors are included. The choice is a common form factor for all components of the current with the dipole form,

$$F(t) = \frac{\Lambda_{\rm EM}^4}{(\Lambda_{\rm EM}^2 - t)^2}. \tag{B4}$$

The integrals can be given analytically, rendering very large expressions. They are obtained through the following steps. One first expresses the form factor as the derivative of a monopole,

$$F(t) = -\Lambda_{\rm EM}^4 \frac{\partial}{\partial a}\frac{1}{a-t}\bigg|_{a\to\Lambda_{\rm EM}^2}. \tag{B5}$$

The momentum transfer at the EM vertices in the box diagram are $t = -2kK(1-\hat{\boldsymbol{k}}\cdot\hat{\boldsymbol{K}})$ and $t' = -2k'K(1-\hat{\boldsymbol{k}}'\cdot\hat{\boldsymbol{K}})$, where k and K, and k' and K, are the moduli of the electron 3-momenta entering in the respective vertices. The box integrals involving the form factors are of the general form, where Pol indicates polynomial in the arguments:

$$\int d\Omega_K \frac{\Lambda_{\rm EM}^8 \mathrm{Pol}(\hat{\boldsymbol{k}}\cdot\hat{\boldsymbol{K}}, \hat{\boldsymbol{k}}'\cdot\hat{\boldsymbol{K}}, \hat{\boldsymbol{K}}^i)}{(1-\hat{\boldsymbol{k}}\cdot\hat{\boldsymbol{K}}+\epsilon)[\Lambda_{\rm EM}^2+2kK(1-\hat{\boldsymbol{k}}\cdot\hat{\boldsymbol{K}})]^2(1-\hat{\boldsymbol{k}}'\cdot\hat{\boldsymbol{K}})[\Lambda_{\rm EM}^2+2k'K(1-\hat{\boldsymbol{k}}'\cdot\hat{\boldsymbol{K}})]^2}$$
$$= \frac{\Lambda_{\rm EM}^8}{(4kk'K^2)^2}\frac{\partial}{\partial a}\frac{\partial}{\partial a'}\int d\Omega_K \frac{\mathrm{Pol}(\hat{\boldsymbol{k}}\cdot\hat{\boldsymbol{K}}, \hat{\boldsymbol{k}}'\cdot\hat{\boldsymbol{K}}, \hat{\boldsymbol{K}}^i)}{(1-\hat{\boldsymbol{k}}\cdot\hat{\boldsymbol{K}}+\epsilon)(1-\hat{\boldsymbol{k}}'\cdot\hat{\boldsymbol{K}}+\epsilon)(a-\hat{\boldsymbol{k}}\cdot\hat{\boldsymbol{K}})(a'-\hat{\boldsymbol{k}}'\cdot\hat{\boldsymbol{K}})}\bigg|_{a^{(\prime)}\to 1+\frac{\Lambda_{\rm EM}^2}{2k^{(\prime)}K}}. \tag{B6}$$

Using partial fractions

$$\frac{1}{(1-\hat{\boldsymbol{k}}\cdot\hat{\boldsymbol{K}}+\epsilon)(a-\hat{\boldsymbol{k}}\cdot\hat{\boldsymbol{K}})} = \frac{1}{a-1}\left(\frac{1}{1-\hat{\boldsymbol{k}}\cdot\hat{\boldsymbol{K}}+\epsilon}+\frac{1}{a-\hat{\boldsymbol{k}}\cdot\hat{\boldsymbol{K}}}\right) \tag{B7}$$

reduces the integrals to be calculated to the general form

$$\int d\Omega_K \frac{\mathrm{Pol}(\hat{\boldsymbol{k}}\cdot\hat{\boldsymbol{K}}, \hat{\boldsymbol{k}}'\cdot\hat{\boldsymbol{K}}, \hat{\boldsymbol{K}}^i)}{(a-\hat{\boldsymbol{k}}\cdot\hat{\boldsymbol{K}}+\epsilon)(a'-\hat{\boldsymbol{k}}'\cdot\hat{\boldsymbol{K}}+\epsilon)}, \tag{B8}$$

where $a, a' \geq 1$. By expanding the numerator these integrals can be reduced to integrals with single or double denominators. The integrals with single denominators are these:

$$\begin{aligned}\boldsymbol{J}(a,n) &= \int d\Omega_K \frac{(\hat{\boldsymbol{k}}\cdot\hat{\boldsymbol{K}})^n}{a-\hat{\boldsymbol{k}}\cdot\hat{\boldsymbol{K}}+\epsilon},\\ &= 2\pi\left(a^n \log\left(\frac{a+1}{a-1+\epsilon}\right) - 2\sum_{m=0}^{\frac{[n-1]}{2}}\frac{a^{n-1-2m}}{2m+1}\right),\\ \boldsymbol{J}^i(\hat{\boldsymbol{k}},a,n) &= \int d\Omega_K \frac{\hat{\boldsymbol{K}}^i(\hat{\boldsymbol{k}}\cdot\hat{\boldsymbol{K}})^n}{a-\hat{\boldsymbol{k}}\cdot\hat{\boldsymbol{K}}+\epsilon}\\ &= \hat{\boldsymbol{k}}^i \boldsymbol{J}(a,n),\end{aligned} \tag{B9}$$

$$\begin{aligned}\boldsymbol{J}^{ij}(\hat{\boldsymbol{k}},a,n) &= \int d\Omega_K \frac{\hat{\boldsymbol{K}}^i\hat{\boldsymbol{K}}^j(\hat{\boldsymbol{k}}\cdot\hat{\boldsymbol{K}})^n}{a-\hat{\boldsymbol{k}}\cdot\hat{\boldsymbol{K}}+\epsilon},\\ &= \frac{1}{2}\{\delta^{ij}[\boldsymbol{J}(a,n)-\boldsymbol{J}(a,n+2)]\\ &\quad +\hat{\boldsymbol{k}}^i\hat{\boldsymbol{k}}^j[3\boldsymbol{J}(a,n+2)-\boldsymbol{J}(a,n)]\}.\end{aligned} \tag{B10}$$

The integrals with double denominators are these:

$$\boldsymbol{J}(\hat{\boldsymbol{k}},\hat{\boldsymbol{k}}',a,a',n,n') = \int d\Omega_K \frac{(\hat{\boldsymbol{k}}\cdot\hat{\boldsymbol{K}})^n(\hat{\boldsymbol{k}}'\cdot\hat{\boldsymbol{K}})^{n'}}{(a-\hat{\boldsymbol{k}}\cdot\hat{\boldsymbol{K}}+\epsilon)(a'-\hat{\boldsymbol{k}}'\cdot\hat{\boldsymbol{K}}+\epsilon)}, \tag{B11}$$

$$\boldsymbol{J}^i(\hat{\boldsymbol{k}},\hat{\boldsymbol{k}}',a,a',n,n') = \int d\Omega_K \frac{\hat{\boldsymbol{K}}^i(\hat{\boldsymbol{k}}\cdot\hat{\boldsymbol{K}})^n(\hat{\boldsymbol{k}}'\cdot\hat{\boldsymbol{K}})^{n'}}{(a-\hat{\boldsymbol{k}}\cdot\hat{\boldsymbol{K}}+\epsilon)(a'-\hat{\boldsymbol{k}}'\cdot\hat{\boldsymbol{K}}+\epsilon)}, \tag{B12}$$

$$\boldsymbol{J}^{ij}(\hat{\boldsymbol{k}},\hat{\boldsymbol{k}}',a,a',n,n') = \int d\Omega_K \frac{\hat{\boldsymbol{K}}^i\hat{\boldsymbol{K}}^j(\hat{\boldsymbol{k}}\cdot\hat{\boldsymbol{K}})^n(\hat{\boldsymbol{k}}'\cdot\hat{\boldsymbol{K}})^{n'}}{(a-\hat{\boldsymbol{k}}\cdot\hat{\boldsymbol{K}}+\epsilon)(a'-\hat{\boldsymbol{k}}'\cdot\hat{\boldsymbol{K}}+\epsilon)}. \tag{B13}$$

Explicit results are shown in the following tables, where $A(a,a',\theta) \equiv \sqrt{a^2a'^2-2aa'\cos\theta-\sin^2\theta}$:

n	n'	$\boldsymbol{J}(\hat{\boldsymbol{k}},\hat{\boldsymbol{k}}',a,a',n,n')$
0	0	$\frac{2\pi}{A(a,a',\theta)}\left(\log\frac{2\sin^2\frac{\theta}{2}-a(a-a')+A(a,a',\theta)}{2\sin^2\frac{\theta}{2}-a(a-a')-A(a,a',\theta)}+a\leftrightarrow a'\right)$
1	0	$a\boldsymbol{J}(\hat{\boldsymbol{k}},\hat{\boldsymbol{k}}',a,a',0,0)-\boldsymbol{J}(a',0)$
1	1	$4\pi+aa'\boldsymbol{J}(\hat{\boldsymbol{k}},\hat{\boldsymbol{k}}',a,a',0,0)-a\boldsymbol{J}(a,0)-a'\boldsymbol{J}(a',0)$
2	0	$a\boldsymbol{J}(\hat{\boldsymbol{k}},\hat{\boldsymbol{k}}',a,a',1,0)-\cos\theta\boldsymbol{J}(a',0)$

(B14)

$$\boldsymbol{J}^i(\hat{\boldsymbol{k}},\hat{\boldsymbol{k}}',a,a',n,n') = -\csc^2\theta\,[(\cos\theta\hat{\boldsymbol{k}}^i-\hat{\boldsymbol{k}}'^i)\boldsymbol{J}(\hat{\boldsymbol{k}},\hat{\boldsymbol{k}}',a,a',n,n'+1)+(\cos\theta\hat{\boldsymbol{k}}'^i-\hat{\boldsymbol{k}}^i)\boldsymbol{J}(k,k',a,a',n+1,n')], \tag{B15}$$

$$\begin{aligned}\boldsymbol{J}^{ij}(\hat{\boldsymbol{k}},\hat{\boldsymbol{k}}',a,a',n,n') &= \delta^{ij}\{\boldsymbol{J}(\hat{\boldsymbol{k}},\hat{\boldsymbol{k}}',a,a',n,n')-\csc^2\theta[-2\cos\theta\boldsymbol{J}(\hat{\boldsymbol{k}},\hat{\boldsymbol{k}}',a,a',n+1,n'+1)+\boldsymbol{J}(\hat{\boldsymbol{k}},\hat{\boldsymbol{k}}',a,a',n,n'+2)\\ &\quad +\boldsymbol{J}(\hat{\boldsymbol{k}},\hat{\boldsymbol{k}}',a,a',n+2,n')]\}+\csc^4\theta\{\hat{\boldsymbol{k}}^i\hat{\boldsymbol{k}}^j[-\sin^2\theta\boldsymbol{J}(\hat{\boldsymbol{k}},\hat{\boldsymbol{k}}',a,a',n,n')+(\cos^2\theta+1)\boldsymbol{J}(\hat{\boldsymbol{k}},\hat{\boldsymbol{k}}',a,a',n,n'+2)\\ &\quad -4\cos\theta\boldsymbol{J}(\hat{\boldsymbol{k}},\hat{\boldsymbol{k}}',a,a',n+1,n'+1)+2\boldsymbol{J}(\hat{\boldsymbol{k}},\hat{\boldsymbol{k}}',a,a',n+2,n')]+\{k,a,n\}\leftrightarrow\{k',a',n'\}\}\\ &\quad +\csc^4\theta(\hat{\boldsymbol{k}}'^i\hat{\boldsymbol{k}}^j+\hat{\boldsymbol{k}}^i\hat{\boldsymbol{k}}'^j)\{(3\cos^2\theta+1)\boldsymbol{J}(\hat{\boldsymbol{k}},\hat{\boldsymbol{k}}',a,a',n+1,n'+1)+\cos\theta\sin^2\theta\boldsymbol{J}(\hat{\boldsymbol{k}},\hat{\boldsymbol{k}}',a,a',n,n')\\ &\quad -2\cos\theta[\boldsymbol{J}(\hat{\boldsymbol{k}},\hat{\boldsymbol{k}}',a,a',n,n'+2)+\boldsymbol{J}(\hat{\boldsymbol{k}},\hat{\boldsymbol{k}}',a,a',n+2,n')]\}.\end{aligned} \tag{B16}$$

APPENDIX C: SPIN-INDEPENDENT OPE CROSS SECTION

This appendix presents the explicit expression of the OPE cross section for elastic scattering $eN \to eN$, which is used as a denominator in the calculation of the TSSA in this work. The OPE cross section is given by[6]

$$\frac{d\sigma_U}{d\Omega} = \frac{\alpha^2}{4m_N^2 s t^2}\left\{\left[G_E^2(4m_N^2 - t) + \frac{2}{\Lambda}G_E G_M m_N t\right][(s-m_N^2)^2 + st] - \frac{1}{\Lambda^2}G_M^2 m_N^2 t[(s-m_N^2)^2 + st - 2m_N^2 t]\right\}, \tag{C1}$$

where Λ is the generic mass scale accompanying the magnetic form factors introduced in Sec. II B. When used in the context of the $1/N_c$ expansion, Eq. (C1) is expanded to the corresponding order in the nonrelativistic expansion. The cross section for general N_c is obtained by replacing in Eq. (C1)

$$G_E \equiv G_E(I_3) = G_E^S + 2I_3 G_E^V, \qquad G_M \equiv G_M(I_3) = G_M^S + \frac{2}{5}I_3(N_c+2)G_M^V, \tag{C2}$$

where G_E^S, etc. are the isoscalar and isovector physical form factors, Eq. (12), and $I_3 = \pm\frac{1}{2}$ is the isospin projection of the initial nucleon state. Then, the strict $1/N_c$ expansion is performed with the scaling assignments $m_N = \mathcal{O}(N_c)$, $\Lambda = \mathcal{O}(N_c^0)$, $\sqrt{s} - m_N = \mathcal{O}(N_c^0)$, and $t = \mathcal{O}(N_c^0)$.

APPENDIX D: SPIN-DEPENDENT TPE CROSS SECTION

This appendix presents the results for the spin-dependent interference cross section the c.m. frame, Eq. (22), for the case where the form factors and the Δ width are ignored. The expressions display separately the contributions where the final and intermediate baryon states are N or Δ. The notation $(N_\mathrm{i}, B_\mathrm{f}, B_\mathrm{n})$ indicates the initial nucleon $N_\mathrm{i} = p$, n with isospin projection $I_3 = \pm\frac{1}{2}$, the final baryon $B_\mathrm{f} = N, \Delta$ and the intermediate baryon $B_\mathrm{n} = N, \Delta$.

$$\begin{aligned}
\frac{d\sigma_N}{d\Omega}(N_\mathrm{i}, N, N) &= \frac{\alpha^3 k^2 m_N^3}{4000\Lambda^3 s^{3/2} t(1+x)}\left[2(1+x) - (x+3)\log\frac{1-x}{2}\right][(N_c-3)G_M(-I_3) - (N_c+7)G_M(I_3)]^2\{10\Lambda G_E(I_3) \\
&\quad + k[(N_c-3)G_M(-I_3) - (N_c+7)G_M(I_3)]\}, \\
\frac{d\sigma_N}{d\Omega}(N_\mathrm{i}, N, \Delta) &= \frac{\Theta(k_\Delta)\alpha^3 m_N^2 m_\Delta}{2000\Lambda^3 s^{3/2} t(1+x)}(N_c-1)(N_c+5)[G_M(-I_3) - G_M(I_3)]^2 \\
&\quad \times\left\{2kk_\Delta(1+x) - \log\frac{1-x}{2}[k^2(1+x) + 2k_\Delta^2]\right\}\{k[(N_c-3)G_M(-I_3) - (N_c+7)G_M(I_3)] - 5\Lambda G_E(I_3)\}, \\
\frac{d\sigma_N}{d\Omega}(N_\mathrm{i}, \Delta, N) &= \frac{\Theta(k_\Delta)\alpha^3 k_\Delta m_N^2 m_\Delta}{16000\Lambda^3 s^{3/2} t(1+x)}(N_c-1)(N_c+5)[G_M(-I_3) - G_M(I_3)]^2\Big(2\log\frac{1-x}{2}\{20\Lambda G_E(I_3)[2k - k_\Delta(1+x)] \\
&\quad - [(N_c-3)G_M(-I_3) - (N_c+7)G_M(I_3)][2k^2 - 3kk_\Delta(x-1) - 2k_\Delta^2(x-2)]\} - (1+x) \\
&\quad \times\{(11k^2 - kk_\Delta + 4k_\Delta^2)[(N_c-3)G_M(-I_3) - (N_c+7)G_M(I_3)] - 40\Lambda G_E(I_3)(k-k_\Delta)\}\Big), \\
\frac{d\sigma_N}{d\Omega}(N_\mathrm{i}, \Delta, \Delta) &= \frac{\Theta(k_\Delta)\alpha^3 k_\Delta^2 m_N^2 m_\Delta}{80000k\Lambda^3 s^{3/2} t(1+x)}(N_c-1)(N_c+5)[G_M(-I_3) - G_M(I_3)]^2 \\
&\quad \times\Big(200\Lambda G_E(I_3)\Big\{(1+x)(k-k_\Delta) + \log\frac{1-x}{2}[k(1+x) - 2k_\Delta]\Big\} \\
&\quad + [(N_c-23)G_M(-I_3) - (N_c+27)G_M(I_3)] \\
&\quad \times\Big\{2\log\frac{1-x}{2}[-6k^2 + kk_\Delta(5x+3) - 6k_\Delta^2] + k_\Delta(1+x)(9k - 23k_\Delta)\Big\}\Big).
\end{aligned} \tag{D1}$$

Here $x \equiv \cos\theta$; k and k_Δ are the c.m. momenta in eN and $e\Delta$ states given by Eq. (8), and $t = -2k_\mathrm{i}k_\mathrm{f}(1-x)$ in each of the above expressions, with $k_\mathrm{i} = k$ and $k_\mathrm{f} = k$ or k_Δ depending on the final baryon state. $G_{M,E}(I_3)$ are the form factors for initial nucleon isospin projection I_3 given by Eq. (C2). Since the above expressions are for the case where the momentum dependence of the form factors is neglected, $G_E^p = 1$ and $G_E^n = 0$.

[6]This is the cross section in terms of the form factors $G_E = F_1$ and $G_M = F_1 + F_2$.

The expansion in $1/N_c$ of the cross sections Eq. (D1) is easily performed using the scaling of the masses as $m_N = \mathcal{O}(N_c)$, $m_\Delta - m_N = \mathcal{O}(N_c^{-1})$, and $\Lambda = \mathcal{O}(N_c^0)$ (to be chosen equal to the physical nucleon mass). For the scaling of the c.m. momentum k there are the three distinguished regimes described in Sec. III A: the low-energy elastic regime, where the energy is below the Δ threshold and $k = \mathcal{O}(N_c^{-1})$; the low-energy inelastic regime, where the energy is above the Δ threshold and $k = \mathcal{O}(N_c^{-1})$; and the intermediate-energy inelastic regime where $k = \mathcal{O}(N_c^0)$. The expressions Eq. (D1) cover all three regimes and can be expanded further with the appropriate scaling assignment for the momenta in each regime.

APPENDIX E: IMPLEMENTATION OF Δ WIDTH

This appendix describes the implementation of the Δ width in the context of the present approach based on the $1/N_c$ expansion. The decay width of the Δ is a quantity $\mathcal{O}(N_c^{-2})$, it however plays an important role in the shape of the asymmetry as the electron energy is near the excitation energy of the Δ. A Breit-Wigner form is used, which leads to the following convolution (smearing) in the calculation of the absorptive part of the box diagram. At vanishing width the integrals in the absorptive part are of the following general form:

$$\int \frac{d^4K}{(2\pi)^4}\,\delta^+(K^2)\,\delta(p^0+q^0-\Delta m)\,\frac{\mathrm{Pol}(K)}{q^2 q'^2}, \tag{E1}$$

where q, q' are the photon momenta in the box, and Δm the $N-\Delta$ mass difference. With finite width Γ the corresponding integral becomes

$$\frac{1}{4\,\arctan\frac{2Q}{\Gamma}}\int_{-Q}^{Q} d\mu\,\frac{\Gamma}{\mu^2+\frac{\Gamma^2}{4}}\int\frac{d^4K}{(2\pi)^4}\,\delta^+(K^2) \times \delta(p^0+q^0-(\Delta m-\mu))\,\frac{\mathrm{Pol}(K)}{q^2 q'^2}. \tag{E2}$$

The domain of integration in μ must be limited by the scale Q, as otherwise the result diverges for large $|\mu|$. It is also logical that $|\mu| < \Delta m$. Results have little sensitivity to Q as far as $\Gamma < Q < \Delta m$. The factor in front of the above expression provides the proper normalization for the convolution.

The end result is that the implementation of the Δ width in the interference cross section is simply given by a smearing of the cross section as follows:

$$d\sigma_N(N,B_\mathrm{f},B_\mathrm{n}) \to \frac{1}{4\,\arctan\frac{2Q}{\Gamma}}\int_{-Q}^{Q} d\mu\,\frac{\Gamma}{\mu^2+\frac{\Gamma^2}{4}} \times d\sigma_N(N,B_\mathrm{f},B_\mathrm{n})|_{m_\Delta\to m_\Delta-\mu}. \tag{E3}$$

[1] M. K. Jones *et al.* (Jefferson Lab Hall A Collaboration), G_{Ep}/G_{Mp} Ratio by Polarization Transfer in $\vec{e}p \to e\vec{p}$, Phys. Rev. Lett. **84**, 1398 (2000).

[2] P. A. M. Guichon and M. Vanderhaeghen, How to Reconcile the Rosenbluth and the Polarization Transfer Method in the Measurement of the Proton Form-Factors, Phys. Rev. Lett. **91**, 142303 (2003).

[3] P. G. Blunden, W. Melnitchouk, and J. A. Tjon, Two Photon Exchange and Elastic Electron Proton Scattering, Phys. Rev. Lett. **91**, 142304 (2003).

[4] B. S. Henderson *et al.* (OLYMPUS Collaboration), Hard Two-Photon Contribution to Elastic Lepton-Proton Scattering Determined by the OLYMPUS Experiment, Phys. Rev. Lett. **118**, 092501 (2017).

[5] J. C. Bernauer *et al.* (OLYMPUS Collaboration), Measurement of the Charge-Averaged Elastic Lepton-Proton Scattering Cross Section by the OLYMPUS Experiment, Phys. Rev. Lett. **126**, 162501 (2021).

[6] A. Accardi *et al.*, An experimental program with high duty-cycle polarized and unpolarized positron beams at Jefferson Lab, Eur. Phys. J. A **57**, 261 (2021).

[7] A. V. Afanasev and C. E. Carlson, Two-Photon-Exchange Correction to Parity-Violating Elastic Electron-Proton Scattering, Phys. Rev. Lett. **94**, 212301 (2005).

[8] A. O. Barut and C. Fronsdal, Spin-orbit correlations in $\mu - e$ and $e^- - e^-$ scattering, Phys. Rev. **120**, 1871 (1960).

[9] J. Arafune and Y. Shimizu, Proton polarization in elastic electron-proton scattering, Phys. Rev. D **1**, 3094 (1970).

[10] U. Guenther and R. Rodenberg, Polarization of the recoil protons in the elastic electron-proton scattering process, Nuovo Cimento A **2**, 25 (1971).

[11] J. P. Leroy and C. A. Piketty, Asymmetry in inelastic electron-polarized proton scattering, Nucl. Phys. **B38**, 466 (1972).

[12] A. De Rujula, J. M. Kaplan, and E. De Rafael, Elastic scattering of electrons from polarized protons and inelastic electron scattering experiments, Nucl. Phys. **B35**, 365 (1971).

[13] B. Pasquini and M. Vanderhaeghen, Resonance estimates for single spin asymmetries in elastic electron-nucleon scattering, Phys. Rev. C **70**, 045206 (2004).

[14] O. Koshchii and A. Afanasev, Target-normal single-spin asymmetry in elastic electron-nucleon scattering, Phys. Rev. D **98**, 056007 (2018).

[15] T. Powell *et al.*, Measurement of the Polarization in Elastic Electron-Proton Scattering, Phys. Rev. Lett. **24**, 753 (1970).

[16] A. Metz, M. Schlegel, and K. Goeke, Transverse single spin asymmetries in inclusive deep-inelastic scattering, Phys. Lett. B **643**, 319 (2006).

[17] A. Afanasev, M. Strikman, and C. Weiss, Transverse target spin asymmetry in inclusive DIS with two-photon exchange, Phys. Rev. D **77**, 014028 (2008).

[18] A. Metz, D. Pitonyak, A. Schafer, M. Schlegel, W. Vogelsang, and J. Zhou, Single-spin asymmetries in inclusive deep inelastic scattering and multiparton correlations in the nucleon, Phys. Rev. D **86**, 094039 (2012).

[19] M. Schlegel, Partonic description of the transverse target single-spin asymmetry in inclusive deep-inelastic scattering, Phys. Rev. D **87**, 034006 (2013).

[20] A. Airapetian *et al.* (HERMES Collaboration), Search for a two-photon exchange contribution to inclusive deep-inelastic scattering, Phys. Lett. B **682**, 351 (2010).

[21] J. Katich *et al.*, Measurement of the Target-Normal Single-Spin Asymmetry in Deep-Inelastic Scattering from the Reaction $^3\mathrm{He}^{\uparrow}(e,e')X$, Phys. Rev. Lett. **113**, 022502 (2014).

[22] Y. W. Zhang *et al.*, Measurement of the Target-Normal Single-Spin Asymmetry in Quasielastic Scattering from the Reaction $^3\mathrm{He}^{\uparrow}(e,e')$, Phys. Rev. Lett. **115**, 172502 (2015).

[23] E. Long *et al.*, Measurement of the single-spin asymmetry A_y^0 in quasi-elastic $^3\mathrm{He}^{\uparrow}(e,e'n)$ scattering at $0.4 < Q^2 < 1.0\ \mathrm{GeV}/c^2$, Phys. Lett. B **797**, 134875 (2019).

[24] G. N. Grauvogel, T. Kutz, and A. Schmidt, Target-normal single spin asymmetries measured with positrons, Eur. Phys. J. A **57**, 213 (2021).

[25] C. E. Carlson and M. Vanderhaeghen, Two-photon physics in hadronic processes, Annu. Rev. Nucl. Part. Sci. **57**, 171 (2007).

[26] G. 't Hooft, A planar diagram theory for strong interactions, Nucl. Phys. **B72**, 461 (1974).

[27] E. Witten, Baryons in the $1/N$ expansion, Nucl. Phys. **B160**, 57 (1979).

[28] J.-L. Gervais and B. Sakita, Large-N QCD Baryon Dynamics: Exact Results from Its Relation to the Static Strong Coupling Theory, Phys. Rev. Lett. **52**, 87 (1984).

[29] J.-L. Gervais and B. Sakita, Large-N baryonic soliton and quarks, Phys. Rev. D **30**, 1795 (1984).

[30] R. F. Dashen and A. V. Manohar, Baryon-pion couplings from large-N_c QCD, Phys. Lett. B **315**, 425 (1993).

[31] R. F. Dashen, E. E. Jenkins, and A. V. Manohar, $1/N_c$ expansion for baryons, Phys. Rev. D **49**, 4713 (1994); **51**, 2489(E) (1995).

[32] R. F. Dashen, E. E. Jenkins, and A. V. Manohar, Spin flavor structure of large N_c baryons, Phys. Rev. D **51**, 3697 (1995).

[33] E. E. Jenkins, Large-N_c baryons, Annu. Rev. Nucl. Part. Sci. **48**, 81 (1998).

[34] I. P. Fernando and J. L. Goity, $SU(3)$ vector currents in baryon chiral perturbation theory combined with the $1/N_c$ expansion, Phys. Rev. D **101**, 054026 (2020).

[35] E. E. Jenkins, X. Ji, and A. V. Manohar, $\Delta \to N\gamma$ in Large-N_c QCD, Phys. Rev. Lett. **89**, 242001 (2002).

[36] J. Dai, R. F. Dashen, E. E. Jenkins, and A. V. Manohar, Flavor symmetry breaking in the $1/N_c$ expansion, Phys. Rev. D **53**, 273 (1996).

[37] J. L. Goity, $1/N_c$ countings in baryons, Phys. At. Nucl. **68**, 624 (2005).

[38] Z. Ye, J. Arrington, R. J. Hill, and G. Lee, Proton and neutron electromagnetic form factors and uncertainties, Phys. Lett. B **777**, 8 (2018).

[39] A. Calle Cordon and J. L. Goity, Baryon masses and axial couplings in the combined $1/N_c$ and chiral expansions, Phys. Rev. D **87**, 016019 (2013).

[40] N. N. Scoccola, J. L. Goity, and N. Matagne, Analysis of negative parity baryon photoproduction amplitudes in the $1/N_c$ expansion, Phys. Lett. B **663**, 222 (2008).

[41] J. L. Goity and N. N. Scoccola, Photo-Production of Positive Parity Excited Baryons in the $1/N_c$ Expansion of QCD, Phys. Rev. Lett. **99**, 062002 (2007).

[42] J. L. Goity, C. Weiss, and C. T. Willemyns, Target normal single-spin asymmetry in inclusive electron-nucleon scattering with two-photon exchange: Analysis using $1/N_c$ expansion, Phys. Lett. B **835**, 137580 (2022).

[43] N. Christ and T. D. Lee, Possible Tests of C_{st} and T_{st} Invariances in $l^{\pm} + N \to l^{\pm} + \Gamma$ and $A \to B + e^+ + e^-$, Phys. Rev. **143**, 1310 (1966).

[44] F. E. Low, Bremsstrahlung of very low-energy quanta in elementary particle collisions, Phys. Rev. **110**, 974 (1958).

[45] M. Gorchtein, P. A. M. Guichon, and M. Vanderhaeghen, Beam normal spin asymmetry in elastic lepton-nucleon scattering, Nucl. Phys. **A741**, 234 (2004).

[46] A. V. Afanasev and N. P. Merenkov, Collinear photon exchange in the beam normal polarization asymmetry of elastic electron-proton scattering, Phys. Lett. B **599**, 48 (2004).

[47] M. Gorchtein, Beam normal spin asymmetry in the quasi-RCS approximation, Phys. Rev. C **73**, 055201 (2006).

[48] C. E. Carlson, B. Pasquini, V. Pauk, and M. Vanderhaeghen, Beam normal spin asymmetry for the $ep \to e\Delta(1232)$ process, Phys. Rev. D **96**, 113010 (2017).

[49] O. Koshchii and A. Afanasev, Lepton mass effects for beam-normal single-spin asymmetry in elastic muon-proton scattering, Phys. Rev. D **100**, 096020 (2019).